nature communications

Article

https://doi.org/10.1038/s41467-024-53277-3

The subcortical maternal complex modulates the cell cycle during early mammalian embryogenesis via 14-3-3

Received: 25 February 2024

Accepted: 7 October 2024

Published online: 15 October 2024

Check for updates

Zhuo Han[1,12], Rui Wang[2,3,4,12], Pengliang Chi[1,12], Zihan Zhang[1,12], Ling Min[1,12], Haizhan Jiao[5], Guojin Ou[1,6], Dan Zhou[2,3], Dandan Qin[2,3], Chengpeng Xu[2,3], Zheng Gao[7], Qianqian Qi[6], Jialu Li[1], Yuechao Lu[1,8], Xiang Wang[1,9,10], Jing Chen[11], Xingjiang Yu[2,3], Hongli Hu[5], Lei Li[2,3] ✉ & Dong Deng[1,9,10] ✉

The subcortical maternal complex (SCMC) is essential for safeguarding female fertility in mammals. Assembled in oocytes, the SCMC maintains the cleavage of early embryos, but the underlying mechanism remains unclear. Here, we report that 14-3-3, a multifunctional protein, is a component of the SCMC. By resolving the structure of the 14-3-3-containing SCMC, we discover that phosphorylation of TLE6 contributes to the recruitment of 14-3-3. Mechanistically, during maternal-to-embryo transition, the SCMC stabilizes 14-3-3 protein and contributes to the proper control of CDC25B, thus ensuring the activation of the maturation-promoting factor and mitotic entry in mouse zygotes. Notably, the SCMC establishes a conserved molecular link with 14-3-3 and CDC25B in human oocytes/embryos. This study discloses the molecular mechanism through which the SCMC regulates the cell cycle in early embryos and elucidates the function of the SCMC in mammalian early embryogenesis.

Maternal-effect mutations have become a critical genetic cause of female reproductive diseases. Since the discovery of maternal-effect genes in mammals[1,2], a growing number of mammalian maternal genes have been identified[3,4]. Maternal-effect proteins, which accumulate prior to fertilization, dominate early preimplantation development until embryonic factors take over[5–7]. A fascinating discovery was the identification of the subcortical maternal complex (SCMC), a multiprotein complex originally found to be enriched in the subcortical region of mammalian oocytes and early embryos that performs multifaceted functions[8–10]. Recent clinical studies revealed a strong link between pathogenic mutations in SCMC genes and early embryonic arrest in women experiencing recurrent reproductive failure[11–13]. The SCMC comprises at least three core components, namely maternal antigen that embryos require (MATER), transducin-like enhancer of split6 (TLE6), and factor located in oocytes permitting embryonic development (FLOPED). Loss of any individual core component arrests embryos in the cleavage-stage during mouse embryonic development[1,8,14], highlighting the SCMC's primary role in promoting zygotes to progress beyond the first cell cycles. Notably, human *TLE6*/*MATER* mutations are closely associated with embryonic lethality

[1]Key Laboratory of Birth Defects and Related Disease of Women and Children of MOE, State Key Laboratory of Biotherapy, West China Second University Hospital, Sichuan University, Chengdu, China. [2]State Key Laboratory of Stem Cell and Reproductive Biology, Key Laboratory of Organ Regeneration and Reconstruction, UCAS/IOZ/CAS, Beijing, China. [3]Beijing Institute of Stem Cell and Regenerative Medicine, Beijing, China. [4]Department of Reproductive Medicine, the First People's Hospital of Yunnan Province, Kunming, China. [5]Kobilka Institute of Innovative Drug Discovery, School of Medicine, The Chinese University of Hong Kong (Shenzhen), Shenzhen, China. [6]Clinical laboratory, West China Second University Hospital, Sichuan University, Chengdu, China. [7]Department of Obstetrics and Gynecology, Center for Reproductive Medicine, The Third Affiliated Hospital of Guangzhou Medical University, Guangzhou, China. [8]Department of Reproductive Medicine, West China Second University Hospital, Sichuan University, Chengdu, China. [9]NHC key Laboratory of Chronobiology, Sichuan University, Chengdu, China. [10]Development and Related Diseases of Women and Children Key Laboratory of Sichuan Province, Sichuan University, Chengdu, China. [11]Laboratory of Pediatric Surgery, Department of Pediatric Surgery, West China Hospital, Sichuan University, Chengdu, China. [12]These authors contributed equally: Zhuo Han, Rui Wang, Pengliang Chi, Zihan Zhang, Ling Min. ✉e-mail: lil@ioz.ac.cn; dengd@scu.edu.cn

at early cleavage stage[11–13]. However, the molecular mechanisms underlying the function of the SCMC in regulating the embryonic cell cycle are almost blank.

14-3-3 proteins belong to a highly homologous family of proteins ubiquitously expressed in all eukaryotic cells[15–17]. The remarkable ability of 14-3-3 proteins to bind a wide array of functionally diverse proteins allows them to act as pleiotropic regulators in various cellular processes, such as the cell cycle[18,19], cell apoptosis[20,21], transcription[22], cytoskeletal rearrangement[23] and protein trafficking[24]. Somatic cell cycle regulation is regarded as one of the core functions of 14-3-3 proteins because they function at multiple critical nodes to determine the onset and timing of mitosis in diverse manners[18,19]. Although previous studies have revealed an additional role for individual 14-3-3 proteins in modulating the meiotic assumption of germinal vesicle (GV) oocytes[25] and the G2/M transition in zygotes[26], the role of 14-3-3 in the cell cycle during the maternal-to-embryo transition has not been determined.

Most recently, we performed in vitro reconstitution of the mouse SCMC and reported the cryoelectron microscopy (cryo-EM) structure of the SCMC ternary core complex (also referred to as the "$SCMC_{core}$" hereafter; includes MATER, TLE6, and FLOPED)[27], offering another perspective for studying the molecular function of the SCMC.

Here, we show that 14-3-3 is an SCMC binding partner and verified the endogenous interaction between 14-3-3 and the SCMC in oocytes. We reconstitute the mouse SCMC in complex with 14-3-3γ and determined its cryo-EM structure at 3.0 Å resolution. Specific phosphorylation sites in mouse TLE6 are pivotal for binding 14-3-3 and may facilitate normal early embryonic development. Furthermore, we show that the SCMC preserved the stability of the 14-3-3 protein during the oocyte-to-zygote transition. Maternal loss of the SCMC reduced 14-3-3 protein levels, while 14-3-3 supplementation in TLE6-deficient zygotes partially rescued the blockage of early embryonic development. In addition, we demonstrate that 14-3-3 strengthened the molecular connection between the SCMC and the critical cell cycle regulator CDC25B. Loss of the SCMC decreased the protein level of CDC25B and led to reduced activity of CDK1 during the maternal-to-embryo transition, inhibiting the onset of mitosis in mouse zygotes. Remarkably, the addition of CDC25B also partially rescued arrest at the first cell divisions in SCMC-deficient mouse zygotes. Finally, we prove that 14-3-3 is also a component of the human SCMC, which establishes a conserved molecular association with CDC25B in human oocytes/embryos. This finding suggests an evolutionarily conserved mechanism of cell cycle regulation by the SCMC in mammalian early embryonic development. This study highlights the significance of 14-3-3 as a component of the SCMC in regulating the early embryonic cell cycle in mammals from a structural perspective and provides additional details for the molecular mechanism by which the SCMC orchestrates mammalian preimplantation embryogenesis.

Results

14-3-3 is an inherent component of the SCMC in mouse oocytes

The SCMC is a MDa-level supercomplex[8], and many studies have progressively identified additional components of the SCMC beyond the core proteins[28–30]. Recently, we reconstituted the mouse SCMC containing MATER, TLE6, FLOPED, and FILIA in Sf9 cells[27]. Interestingly, the purified SCMC proteins exhibited two adjacent protein peaks upon anion-exchange chromatography (Supplementary Fig. 1a), suggesting the presence of two distinct charge states. In the peak representing more negative charge, two proteins other than MATER, TLE6, FLOPED, and FILIA, with molecular weights ranging from 25-35 kDa, were present. Size-exclusion chromatography further confirmed that these two proteins comigrated with SCMC proteins, and both were identified as 14-3-3 proteins by mass spectrometry analysis (Supplementary Fig. 1b).

To investigate whether 14-3-3 is a component of the SCMC in mouse oocytes, we incubated the purified mouse $SCMC_{core}$ with mouse oocyte lysates in vitro, and performed pull-down assay for the $SCMC_{core}$. The result showed that the $SCMC_{core}$ could bind endogenous 14-3-3 (pan 14-3-3) in mouse oocytes (Supplementary Fig. 1c). Furthermore, we performed coimmunoprecipitation (co-IP) assays with a specific antibody to against MATER, TLE6, or FLOPED. The results showed that endogenous 14-3-3 coprecipitated with all three $SCMC_{core}$ components in oocytes (Fig. 1a). Additionally, the immunofluorescence (IF) staining results revealed that SCMC core components were distributed in cytoplasm and enriched in the subcortical region of mouse oocytes, consistent with the reported localization of Halo-tagged TLE6 in mouse oocytes[31]. The 14-3-3 protein was partially colocalized with $SCMC_{core}$ components in mouse oocytes (Fig. 1b). These results substantiate that 14-3-3 is an inherent component of the SCMC in mouse oocytes.

The overall structure of the mouse 14-3-3-containing SCMC

There are seven known 14-3-3 paralogs in mice (denoted by the Greek letters β/α, γ, ε, η, θ, ζ/δ, and σ, with α and δ representing phosphorylated β and ζ paralogs, respectively)[15–17]; these paralogs are highly conserved in their sequence and functionally redundant. According to the reported proteomic data, all seven 14-3-3 paralogs are detectable in mouse oocytes[32–34]. In line with their virtually identical interaction specificities for the ligands[35–37], all seven mouse 14-3-3 paralogs bound the SCMC to varying degrees, and 14-3-3γ was the most potent binding partner (Supplementary Fig. 1d). Thus, we reconstituted the 14-3-3γ-containing SCMC (also referred to as "SCMC-14-3-3γ" hereafter) in vitro by size-exclusion chromatography. Notably, 14-3-3γ comigrated with the SCMC, and the reconstituted SCMC-14-3-3γ exhibited monodisperse behavior (Fig. 1c). Furthermore, we determined the cryo-EM structure of the SCMC-14-3-3γ at a resolution of 3.0 Å (Fig. 1d and Supplementary Figs. 2a–d and 3; Supplementary Table 1). Moreover, 2D classification during data processing also revealed the further dimerization of the SCMC-14-3-3γ (Supplementary Fig. 2a), which is consistent with that of the SCMC[27].

The SCMC-14-3-3γ pentamer comprises MATER, TLE6, FLOPED, and dimeric 14-3-3γ (Fig. 1d). MATER, TLE6, and FLOPED adopt similar conformations in the SCMC-14-3-3γ and the reported structure of the $SCMC_{core}$[27], with a root-mean-square deviation (RMSD) value of 0.768 Å (Supplementary Fig. 4a). Dimeric 14-3-3γ adopts a canonical conformation that resembles the reported crystal structures of 14-3-3 paralogs[38,39] (Fig. 1d and Supplementary Fig. 4a). The two 14-3-3γ protomers (14-3-3γ A and 14-3-3γ B) contact the top surface of the WD40 repeat (WDR) domain of TLE6 and the leucine-rich repeat (LRR) domain of MATER, respectively (Fig. 1e). Notably, there are two additional densities within the ligand-binding clefts of the 14-3-3γ homodimer in the SCMC-14-3-3γ (Fig. 1d). 14-3-3 paralogs are abundant acidic proteins that assemble as homo- or heterodimers and bind phosphorylated ligands through a conserved amphipathic cleft[17]. Therefore, we speculated that two phosphopeptides from SCMC subunits insert into the chamber of 14-3-3γ.

Phosphorylated TLE6 is essential for 14-3-3 recruitment

According to the unsharpened density map, we found that one peptide, TLE6 (133–144) pS139, linked by the MATER-interacting helix (MIH) of TLE6 inserts into the chamber of 14-3-3γ A (Supplementary Fig. 4b). Interestingly, in silico analysis by 14-3-3-Pred[40] revealed that there are three putative 14-3-3 binding sites in the flexible region of the recombinant TLE6 (48–581 aa), including TLE6 (133–144) pS139, TLE6 (203–214) pS209, and TLE6 (217–228) pS223 (Supplementary Fig. 4c). Therefore, we hypothesized that two 14-3-3 binding peptides are derived from TLE6 and tentatively built two phosphopeptides of TLE6, TLE6 (133–144) pS139 and TLE6 (203–214) pS209, in the structure model of the SCMC-14-3-3γ (Fig. 2a–c). The positively charged residues in the grooves of the two 14-3-3γ protomers form direct contacts with phosphorylated Ser139 and Ser209 of TLE6 (Fig. 2a–c).

https://doi.org/10.1038/s41467-024-53277-3

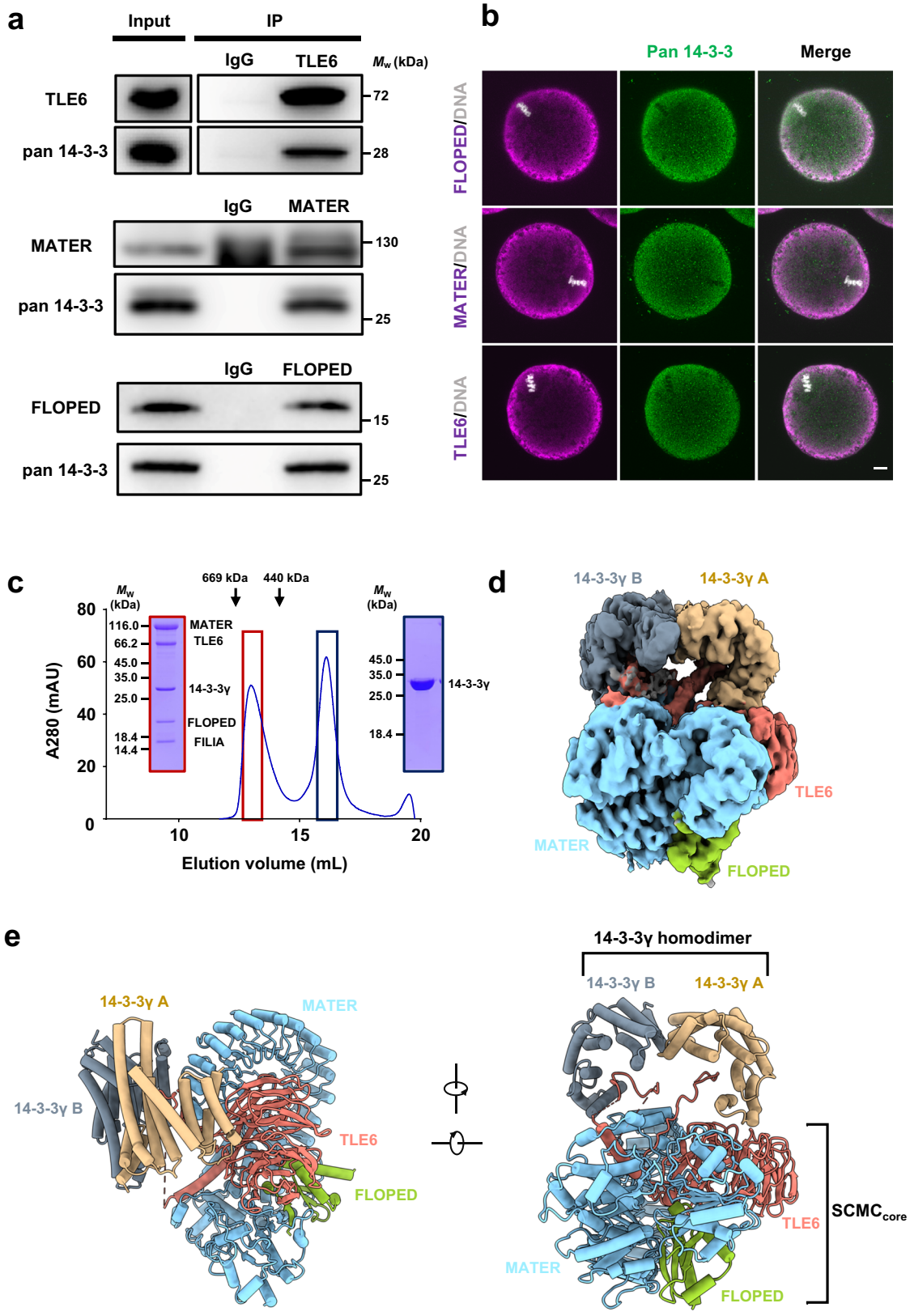

The phosphorylation of protein is vital for 14-3-3 binding[17,18]. Therefore, we introduced the mutations into TLE6 to block the phosphorylation and performed co-IP assays to verify the formation of the 14-3-3-containing SCMC (Fig. 2d). We confirmed that none of the mutations affected the stability of TLE6 and the assembly of the SCMC$_{core}$ (Fig. 2d). Interestingly, TLE6$_{S139A}$ and TLE6$_{S209A}$ weakened the interaction between the SCMC$_{core}$ and 14-3-3γ, with the TLE6$_{S139A}$ having a more significant influence on the binding of 14-3-3γ (Fig. 2d). However, TLE6$_{S223A}$ did not affect the 14-3-3 binding. Notably, TLE6$_{S139/209A}$ and TLE6$_{S139/209/223A}$ also impaired but did not completely disrupt the binding of 14-3-3γ to the SCMC$_{core}$ (Fig. 2d), suggesting the presence of other interfaces between the SCMC$_{core}$ and

Fig. 1 | 14-3-3 exhibits as an SCMC component. a Normal oocyte lysates, before (Input) or after immunoprecipitation with antibody to TLE6 (top), MATER (middle) or FLOPED (bottom) were immunoblotted and probed with antibodies to pan 14-3-3 and TLE6, MATER, or FLOPED, respectively. IgG, normal immunoglobulin (negative control). **b** Normal oocytes isolated from normal females were fixed, permeabilized, and incubated with antibodies to pan 14-3-3 and FLOPED (top), MATER (middle), or TLE6 (bottom), and with DAPI to visualize DNA. The oocytes were imaged by confocal microscopy. Scale bar, 10 μm. Colocalization of pan 14-3-3 and FLOPED, MATER, or TLE6 was presented in the merge. **c** In vitro reconstitution of mouse SCMC-14-3-3γ. The mouse SCMC quaternary complex and 14-3-3γ protein were incubated in lysis buffer. Size-exclusion chromatography (Superose™ 6 Increase 10/300 GL) was performed to separate the SCMC-14-3-3γ (marked in dark red box) and excess 14-3-3γ (marked in dark blue box). The SCMC-14-3-3γ is composed of His-tagged MATER (1–1059 aa), Strep-tagged TLE6 (48–581 aa), Strep-tagged FLOPED (1–164 aa), Strep-tagged FILIA (1–124 aa), and 14-3-3γ (1–247 aa). The column was calibrated with thyroglobulin (669 kDa) and ferritin (440 kDa). **d** Cryo-EM map of the SCMC-14-3-3γ. 14-3-3γ A and 14-3-3γ B refer to two protomers in 14-3-3γ homodimer. MATER, TLE6, and FLOPED are colored in light blue, salmon, and yellow green, respectively. The homodimer of 14-3-3γ is distinguished by 14-3-3γ A (burlywood), which is proximal to the WD40 repeat domain of TLE6, and 14-3-3γ B (gray), which is close to the leucine-rich repeat domain of MATER. The map was shown at level 0.00679. **e** Two views of the cartoon presentation of the SCMC-14-3-3γ structure. The color scheme is consistent with panel **d**. The $SCMC_{core}$ indicates the core complex consisting of MATER, TLE6, and FLOPED.

14-3-3γ. This result is consistent with the structural observation of additional contacts among 14-3-3γ, the LRR domain of MATER, and the WDR domain of TLE6 (Supplementary Fig. 4d-f).

To further illustrate that the phosphorylation of TLE6 at Ser139 and Ser209 contributes to the recruitment of 14-3-3γ, we performed isothermal titration calorimetry assays to measure the binding affinity (K_d) between 14-3-3γ and TLE6 peptides (Fig. 2e and Supplementary Fig. 5). The phosphopeptides, TLE6 (133–144) pS139 and TLE6 (203–214) pS209, were detected to bind to 14-3-3γ with K_d values of 55.8 ± 13.6 μM and 315.3 ± 28.0 μM, respectively. However, two wild-type peptides, TLE6 (133–144) and TLE6 (203–214), and phosphopeptide TLE6 (217–228) pS223 cannot bind to 14-3-3γ. Of note, the mass spectrometry analysis also identified the phosphorylated Ser139 and Ser209 of purified TLE6 in the SCMC-14-3-3 (Supplementary Fig. 6). These findings, together with the results of the co-IP assays, confirmed that the phosphorylation of TLE6 at Ser139 and Ser209 of TLE6 is vital for the binding between 14-3-3γ and SCMC (Fig. 2d). Therefore, we confirmed the model building of SCMC-14-3-3γ.

Next, we combined Trim-Away and mRNA supplementation in mouse zygotes to investigate whether $TLE6_{S139/209A}$ impacts the development of early mouse embryos. At 24, 48, 72, and 96 h post-microinjection (pMI), the developmental rate of zygotes was examined. 94% of the zygotes were 2-cell embryos at 24 h pMI, 93% were 8-cell embryos at 48 h pMI, 95% were morulae at 72 h pMI, and 97% were blastocysts at 96 h pMI in the control group (Fig. 2f and Supplementary Fig. 7a,b). However, TLE6 knockdown in zygotes delayed embryonic development at all time points, with the blastocyst rate being only 6% at 96 h pMI (Fig. 2f and Supplementary Fig. 7a,b). In contrast, this delay in development was partially rescued after supplementation of mRNA encoding wild-type TLE6, with the blastocyst rate rebounding to 62% at 96 h pMI (Fig. 2f and Supplementary Fig. 7a,b). The addition of $TLE6_{S139/209A}$ increased the blastocyst rate to only 32% at 96 h pMI (Fig. 2f and Supplementary Fig. 7a,b). Duncan et al. reported that TLE6 could be phosphorylated by protein kinase A (PKA) in mouse oocytes, with Ser139 and Ser209 sites predicted as high-confidence PKA targets[41]. We thus examined the effect of PKA on the early embryonic development (Supplementary Fig. 8). In the control group, we observed that almost all embryos developed to blastocyst at 120 h post-human chorionic gonadotrophin injection (pHCGi) (Supplementary Fig. 8). In contrast, when subjected to H89, a potent inhibitor of PKA, the progression of early embryonic development was markedly retarded, commencing from 72 h pHCGi. Specifically, the blastocyst formation rate in the H89-treated group plummeted to merely 30% at 120 h pHCGi, with a preponderance of embryos halting their development at the 2-cell stage, exhibiting a phenotypic manifestation akin to SCMC-deficient embryos (Supplementary Fig. 8). While this may provide supporting evidence, the potential off-target effects of the inhibitor and its impact on other potential substrates of PKA cannot be ignored entirely. Additionally, we found that compared with the microinjection of wild-type *Tle6* mRNA, the microinjection of $Tle6_{S139/209A}$ mRNA into normal zygotes resulted in most embryos arresting at the 2-cell stage or death (Supplementary Fig. 7c), similar to the effect of H89 treatment on embryonic development (Supplementary Fig. 8). Despite the potential side effect on normal zygotes, the overexpression of $TLE6_{S139/209A}$, characterized by a markedly diminished capacity to bind with 14-3-3 proteins, may competitively impede the function of the SCMC in maintaining early embryonic development. Taken together, these results indicate that site-specific phosphorylation of TLE6 could promote the recruitment of 14-3-3 to the SCMC in vitro and sustain the normal early embryonic development of mice.

The SCMC maintains early embryogenesis by stabilizing 14-3-3

According to previous reports[42,43], the similar expression patterns of three $SCMC_{core}$ components and six 14-3-3 paralogs across stages ranging from the oocyte stage to the early embryo stage indicates strong positive correlations between SCMC and 14-3-3 expression at the protein level throughout development. Recent proteome analysis by Jentoft et al. revealed that the levels of five 14-3-3 paralogs are reduced in GV oocytes from female $Tle6^{-/-}$ (also referred to as "$Tle6^{Null}$" hereafter; see Methods) mice[31]. In line with these results, we also found that the protein expression level of pan 14-3-3, which was examined by immunoblotting, was significantly lower in GV oocytes from female $Tle6^{Null}$ mice, in comparison to those derived from normal female mice (also referred to as control oocytes hereafter) (Fig. 3a). The IF staining results also confirmed this observation (Fig. 3b and Supplementary Fig. 9a). Ablation of FLOPED, another core component of the SCMC, also markedly attenuated the pan 14-3-3 levels in GV oocytes (Fig. 3c, d and Supplementary Fig. 9b). These results suggest that SCMC maintains the abundance of 14-3-3 proteins in fully grown oocytes. Nonetheless, depletion of the SCMC disrupts the normal cleavage of the mouse embryo after fertilization without affecting the maturation efficiency of the oocyte[1,8,14]. Hence, we tested the possible alteration in the abundance of 14-3-3 in zygotes from female $Tle6^{Null}$ mice. As shown in Fig. 3e, f and Supplementary Fig. 9c, the protein levels of 14-3-3 were significantly lower in zygotes from female $Tle6^{Null}$ mice than those in control zygotes. A similar decrease in pan 14-3-3 protein levels was also observed in zygotes derived from female $Floped^{-/-}$ (also referred to as "$Floped^{Null}$" hereafter) mice (Fig. 3g, h and Supplementary Fig. 9d). These results indicate that the scarcity of 14-3-3 caused by the loss of maternal TLE6, or even of the SCMC, persists from the oocyte stage through the postfertilization stage.

Subsequently, quantitative real-time PCR (qRT-PCR) was also conducted to measure the mRNA levels of 14-3-3 in control, $Tle6^{Null}$ and $Floped^{Null}$ GV oocytes. The results showed that there was no decrease in 14-3-3 mRNA levels between normal and $Tle6^{Null}$ or $Floped^{Null}$ GV oocytes (Supplementary Fig. 10a), suggesting that loss of the SCMC does not reduce the abundance of 14-3-3 proteins by downregulating their mRNA expression. Therefore, we speculated that the mouse SCMC could maintain the stability of 14-3-3 proteins. To support this idea, exogenous mouse 14-3-3γ was gradually degraded in HEK-293F cells by cycloheximide treatment, but this change was significantly inhibited by the preloaded $SCMC_{core}$ despite degradation of the complex itself (Supplementary Fig. 10b). We also found that the

https://doi.org/10.1038/s41467-024-53277-3

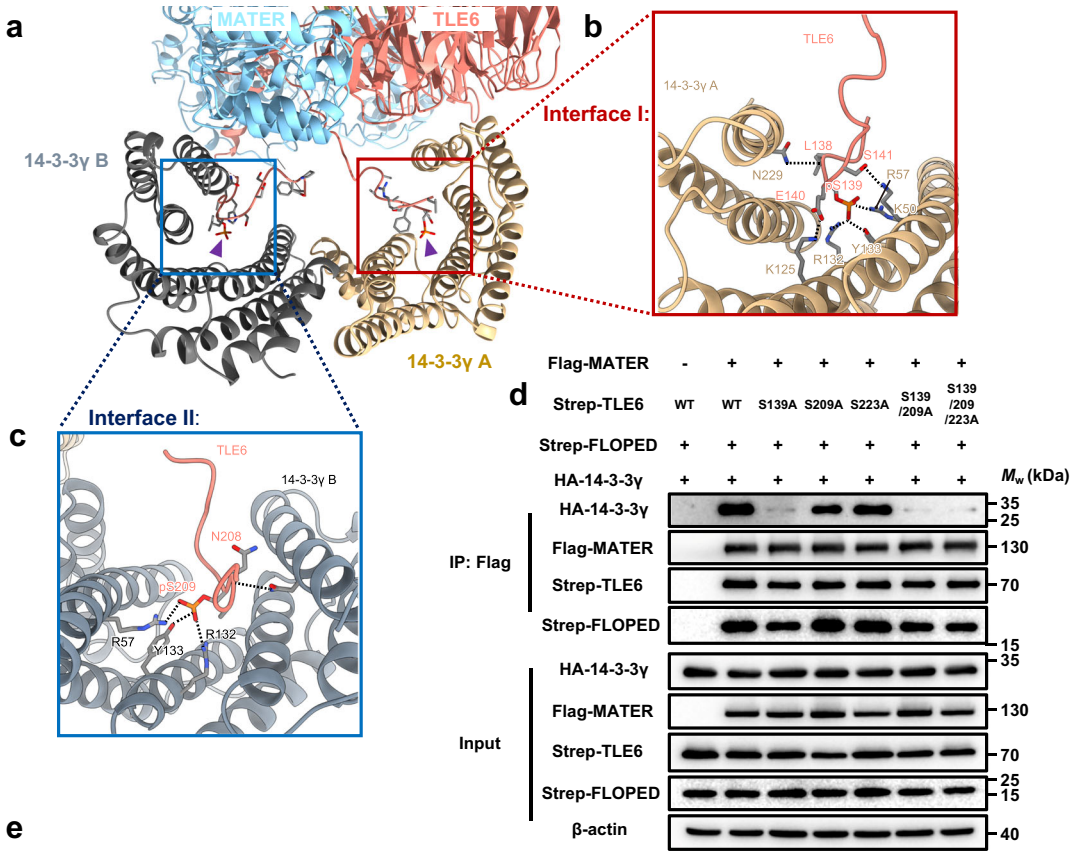

e

Group	TLE6 (133-144) pS139	TLE6 (133-144)	TLE6 (203-214) pS209	TLE6 (203-214)	TLE6 (217-228) pS223	TLE6 (217-228)
K_d	55.8 ± 13.6 μM	UD	315.3 ± 28.0 μM	UD	UD	—

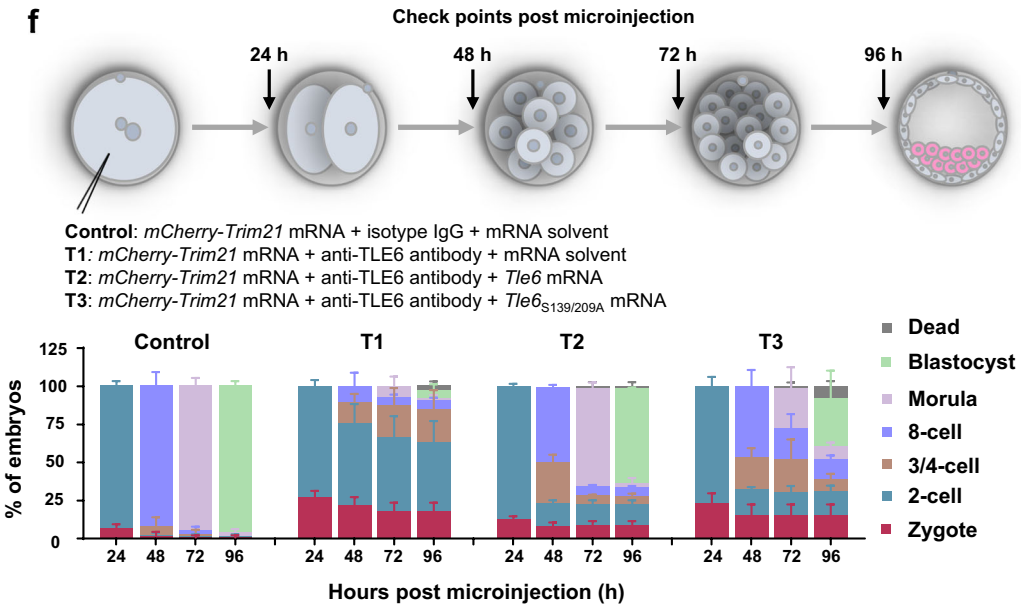

decrease in the protein level of 14-3-3γ could be effectively rescued in HEK-293F cells by incubation with the potent proteasome inhibitor MG132, indicating that mouse 14-3-3γ undergoes proteasomal degradation (Supplementary Fig. 10c). Adding *Tle6* mRNA to TLE6-knockdown zygotes also significantly protected pan 14-3-3 from degradation (Supplementary Fig. 10d). The above results suggest that SCMC stabilizes the 14-3-3 protein levels by preventing 14-3-3 proteins from degradation rather than retaining their mRNA expression.

To investigate whether the reductions in the levels of 14-3-3 proteins are the critical cause of developmental arrest, we knocked down 14-3-3 proteins in normal mouse zygotes and examined their development. The progression of zygote development was significantly

Fig. 2 | Site-specific phosphorylation of TLE6 is important for binding 14-3-3. **a**–**c** Interface I and II mediating the binding of two 14-3-3γ protomers to TLE6 in the SCMC. Interface I (**b**, marked in red box) and Interface II (**c**, marked in blue box) show the interactions of two 14-3-3γ protomers with TLE6 pS139 and pS209, respectively. Purple triangles indicate TLE6 pS139 and pS209, respectively. pS, phosphorylated serine. Single components are colored and labeled as denoted. **d** HEK-293F cells were co-transfected with expression vectors harboring Flag-tagged MATER (or a blank vector for negative control), Strep-tagged FLOPED, HA-tagged 14-3-3γ and either Strep-tagged TLE6, $TLE6_{S139A}$ mutant, $TLE6_{S209A}$ mutant, $TLE6_{S223A}$ mutant, $TLE6_{S139/209A}$ double-site mutant, or $TLE6_{S139/209/223A}$ triple-site mutant as denoted. 60 h after transfection, cell lysates before (Input) or after immunoprecipitation with anti-Flag affinity agarose gel were immunoblotted for HA-tagged 14-3-3γ, Flag-tagged MATER, Strep-tagged FLOPED and Strep-tagged TLE6 (or mutants). **e** Table for binding affinity (K_d) between His-tagged 14-3-3γ and TLE6 wildtype peptides (TLE6 (133–144) or TLE6 (203–214)) or phosphorylated peptides (TLE6 (133–144) pS139, TLE6 (203–214) pS209, or TLE6 (217–228) pS223). The data represent the mean ± S.D. (standard deviation) of 3 independent experiments. pS, phosphorylated serine. UD, undetectable. The minus symbol "-" indicates that the peptide TLE6 (217–228) was undetermined due to insolubility. **f** Schematic overview of mouse zygotes cultured for 24, 48, 72, and 96 h after co-microinjection with *mCherry-Trim21* mRNA + isotype IgG + mRNA solvent (control), *mCherry-Trim21* mRNA + anti-TLE6 antibody + mRNA solvent (T1), *mCherry-Trim21* mRNA + anti-TLE6 antibody + *Tle6* mRNA (T2), or *mCherry-Trim21* mRNA + anti-TLE6 antibody + $Tle6_{S139/209A}$ mRNA (T3). The validation for the loss of TLE6 was presented in Supplementary Fig. 7b. The proportions of embryos on different stages were calculated. $N = 3$ independent experiments. The data are presented as the mean ± S.D.

delayed at all time points in the 14-3-3-knockdown group compared with the control group, with most of the early embryos being arrested at the 2-cell stage at 96 h pMI (Fig. 3i, j, and Supplementary Fig. 11); this was consistent with the abnormal development of TLE6-knockdown zygotes (Fig. 2f and Supplementary Fig. 7a,b). These results suggest that 14-3-3 proteins are crucial for the preimplantation development of mouse embryos.

We then investigated whether 14-3-3 supplementation could rescue the arrested development of early embryos from TLE6-deficient female mice. To this end, the zygotes were isolated from $Tle6^{Null}$ females mated with normal males. These zygotes were injected with mRNA solvent for control or mixed mRNAs containing all seven mouse 14-3-3 paralogs and were subsequently cultured for 96 hours. As expected, control zygotes derived from $Tle6^{Null}$ female mice exhibited delayed development and could not progress beyond the 4-cell stage (Fig. 3k, l), similar to the findings of previous reports[14]. In contrast, upon 14-3-3 supplementation, the proportion of 4-cell embryos from female mice lacking TLE6 dramatically increased by 48 h pMI. Strikingly, after 14-3-3 supplementation, more than 10% of the zygotes from female $Tle6^{Null}$ mice reached the 8-cell stage (Fig. 3k, l). We also found that the developmental defects were partially rescued by 14-3-3 supplementation in TLE6-knockdown zygotes, with the blastocyst rate increasing from 2% to 24% at 96 h pMI (Supplementary Fig. 12). Overall, we conclude that SCMC protects early embryonic development by maintaining 14-3-3 protein levels.

14-3-3 enhances the binding of CDC25B to the SCMC

Oocytes from female mice lacking the SCMC can be fertilized, and the preimplantation development of the resulting zygotes is severely impaired[1,8,14]. According to our previous studies, the time to progress from the 1-cell stage to the 2-cell stage was significantly prolonged in zygotes from female $Tle6^{Null}$ and $Floped^{Null}$ mice, and most of these zygotes eventually stalled at the 2-cell stage[8,14]. These findings strongly suggest that the SCMC is essential for the first cleavage of mouse zygotes. The regulation of cell cycle modulators by 14-3-3 is crucial for coordinating the eukaryotic cell cycle[18,19]. The incorporation of 14-3-3 in the SCMC provides important clues to explain the role of the SCMC in regulating the cell division cycle in zygotes. Therefore, the SCMC may orchestrate the functions of cell cycle factors regulated by 14-3-3.

Previous studies have carefully profiled each phase of the first mitosis in mouse zygotes through 5-ethynyl-2′-deoxyuridine (EdU) labeling[44,45]. To explore how the SCMC functions specifically in the first zygotic cell cycle, we labeled the zygotes with EdU and then examined DNA synthesis and the state of the nucleus in control and $Floped^{Null}$ mouse zygotes after in vitro fertilization (IVF). We considered a EdU signal/total embryo ratio greater than 0.5 to indicate active DNA synthesis. Overall, consistent with the findings of previous studies, almost all the zygotes in the control group exhibited active DNA synthesis between 4-7 h (over 90%) and 7–10 h (100%) post-IVF (Fig. 4a and Supplementary Fig. 13a). Notably, EdU signals did not appear in more than 96% of the control zygotes between 0 and 4 h post-IVF and was abolished in 90% of the control zygotes between 10 and 13 h post-IVF (Fig. 4a and Supplementary Fig. 13a). By comparison, we observed a delayed peak in active DNA synthesis in *Floped*-deficient zygotes between 7–10 h (over 93%) and 10–13 h (100%) post-IVF (Fig. 4a and Supplementary Fig. 13a). We further characterized in detail the timing of active DNA synthesis in control and $Floped^{Null}$ zygotes by splitting the EdU signal peaks into hourly intervals (Supplementary Fig. 13b,c). The results revealed a 4-hour stage of active DNA synthesis between 6 and 10 h post-IVF in control zygotes (Supplementary Fig. 13b); however, the zygotes from female $Floped^{Null}$ mice showed a slightly prolonged duration of active DNA synthesis between 7 and 12 h post-IVF (Supplementary Fig. 13c). Strikingly, most of the control embryos reached the 2-cell stage between 13 and 16 h post-IVF; however, the earliest time point at which the $Floped^{Null}$ zygotes progressed to the 2-cell stage was between 22 and 25 h post-IVF (Fig. 4a and Supplementary Fig. 13a–c). These findings suggest that depletion of FLOPED leads to prolonged cell cycle, especially a markedly delayed G2/M transition, in mouse early embryos.

Cell division cycle 25 homolog B (CDC25B) is pivotal for initiating mitosis in mammalian cells, and its function is tightly controlled by 14-3-3[18,46,47]. Unlike mice lacking *Cdc25a* or *Cdc25c*[48,49], *Cdc25b*-deficient female mice are viable but sterile[50]. Previous studies suggested that CDC25B is the primary CDC25 homolog that participates in the resumption of meiosis[50–52], the metaphase I-to-metaphase II transition[53], and centrosomal microtubule nucleation in 2-cell embryos[54]. Thus, we wondered whether the SCMC and CDC25B are linked through 14-3-3 to regulate the onset of mitosis during the maternal-to-embryo transition. Notably, the results of proximity ligation assays (PLAs) revealed in situ interactions between TLE6 and CDC25B in GV oocytes, mature eggs, and zygotes, suggesting a link between the SCMC and CDC25B in the maternal-to-embryo transition (Fig. 4b). To explore whether 14-3-3 maintains this interaction, we further performed a PLA on 14-3-3-knockdown GV oocytes. The in situ interaction between TLE6 and CDC25B was dramatically impaired in the 14-3-3-knockdown group compared with the control injection group, suggesting an important role for 14-3-3 in promoting CDC25B binding to the SCMC (Fig. 4c). Furthermore, we confirmed the binding of the $SCMC_{core}$ with CDC25B in HEK-293F cells (Fig. 4d). In contrast, the interactions of $TLE6_{S139A}$, $TLE6_{S209A}$, and $TLE6_{S139/S209A}$ with 14-3-3 were significantly inhibited (Fig. 2d), which also compromised their binding with CDC25B (Fig. 4d). Conversely, overexpression of 14-3-3γ in HEK-293F cells significantly promoted the interaction between the $SCMC_{core}$ and CDC25B (Fig. 4e). Taken together, the above analyzes reveal that 14-3-3 mediates and enhances the SCMC-CDC25B association.

The SCMC-14-3-3 stabilizes CDC25B for mitotic entry

14-3-3 binding contributes to the cytoplasmic sequestration of CDC25B[19,46] or protects CDC25B from ubiquitination-mediated

https://doi.org/10.1038/s41467-024-53277-3

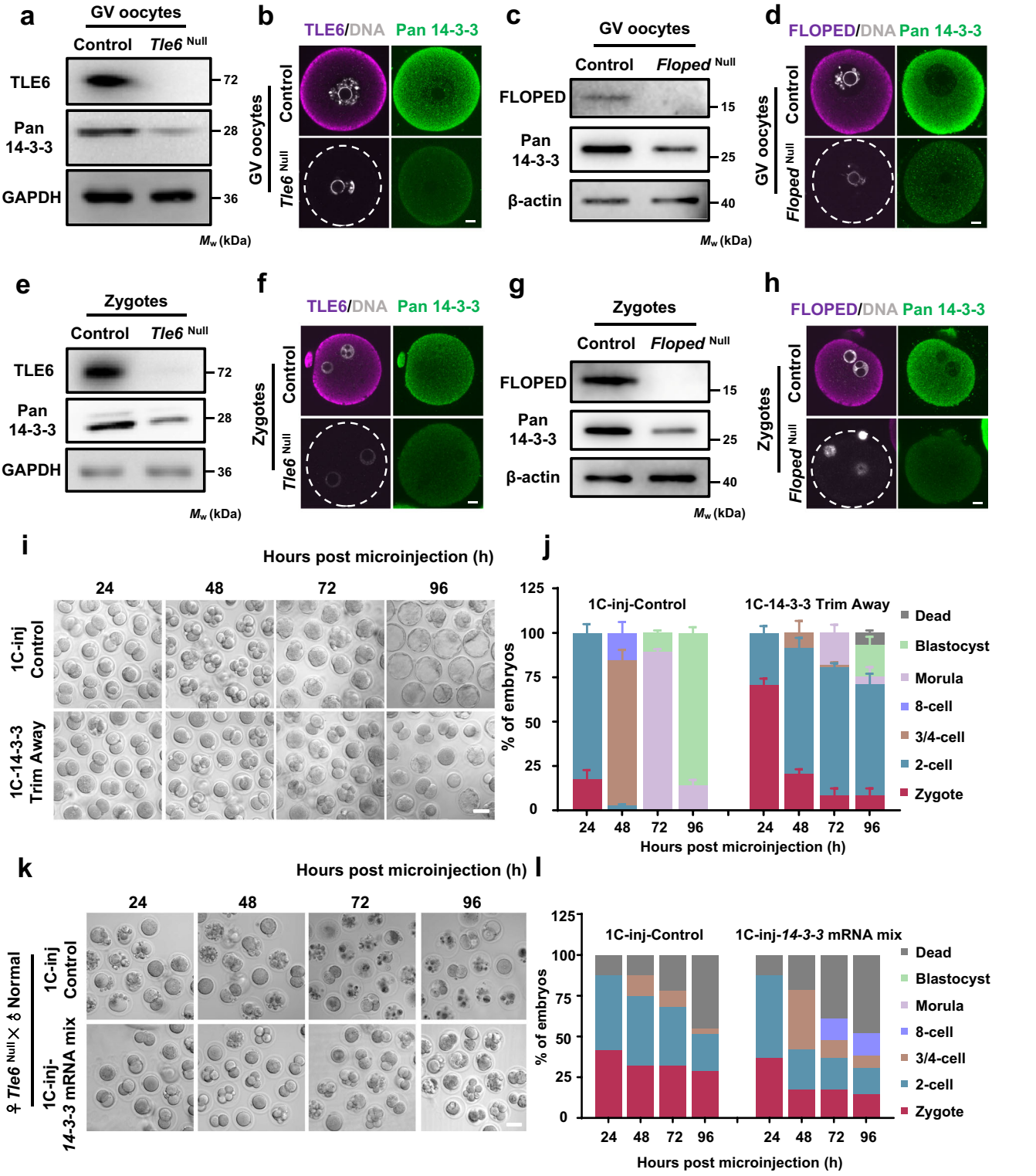

degradation[55]. Given the 14-3-3-mediated connection between the SCMC and CDC25B, we investigated the possible regulatory effect of the SCMC on CDC25B during the maternal-to-embryo transition. As shown in Fig. 5a, b and Supplementary Figs. 14a and 15a,b, the protein level of CDC25B, as determined by immunoblotting and IF staining, was markedly lower in *Tle6*^{Null} GV oocytes than those in control GV oocytes. A similar change in the abundance of CDC25B was observed in GV oocytes from female *Floped*^{Null} mice (Fig. 5c, d and Supplementary Figs. 14b and 15c,d), suggesting that the SCMC rather than a single SCMC component plays a role in controlling CDC25B content. Moreover, we detected no significant changes in the mRNA levels of *Cdc25b* between normal and *Tle6*^{Null} or *Floped*^{Null} GV oocytes (Supplementary Fig. 16), thus ruling out the possibility that the SCMC might regulate the transcription of *Cdc25b*. This indicates that the SCMC directly regulates the stability of the CDC25B protein in fully developed mouse oocytes.

Given that the loss of the SCMC reduces the abundance of 14-3-3 in mouse zygotes (Fig. 3e–h and Supplementary Fig. 9), we further investigated whether CDC25B is also altered in these zygotes. As presented in Fig. 5e, g and Supplementary Figs. 14c and 15e,f, the protein level of

Fig. 3 | The SCMC ensures the storage of 14-3-3 protein and safeguards early embryonic development in mice. a Immunoblotting of 14-3-3 in normal control and *Tle6*^{Null} germinal vesicle (GV) oocytes. **b** Immunofluorescence (IF) staining in GV oocytes isolated from control or *Tle6*^{Null} female mice. Scale bar, 10 μm. **c** Immunoblotting of 14-3-3 in control and *Floped*^{Null} GV oocytes. **d** IF staining in GV oocytes isolated from control or *Floped*^{Null} female mice. Scale bar, 10 μm. **e** Immunoblotting of 14-3-3 in zygotes from control and *Tle6*^{Null} female mice. Zygotes were flushed from the oviduct of female mice that underwent super-ovulation with gonadotrophins and were mated with normal males. **f** GV oocytes isolated from control or *Tle6*^{Null} female mice were cultured to mature eggs and incubated with normal sperms in vitro. After in vitro fertilization (IVF), the resulted zygotes were collected for IF staining. Scale bar, 10 μm. **g** Immunoblotting of 14-3-3 in zygotes from control and *Floped*^{Null} female mice. **h** GV oocytes isolated from control or *Floped*^{Null} female mice were cultured to mature eggs and incubated with normal sperms in vitro. After IVF, the resulted zygotes were collected for IF staining. Scale bar, 10 μm. **i** Representative images of mouse zygotes cultured for 24, 48, 72, and 96 h after co-microinjection with *mCherry-Trim21* mRNA + isotype IgG (control) or *mCherry-Trim21* mRNA + anti-pan 14-3-3 antibody. Scale bar, 50 μm. The validation for the loss of pan 14-3-3 was presented in Supplementary Fig. 11. **j** The proportions of embryos on different stages in panel **i** were calculated. $N = 3$ independent experiments. The data are presented as mean ± S.D. (standard deviation). **k** Representative images of zygotes cultured for 24, 48, 72, and 96 h after microinjection with mRNA solvent (control) or mixed mRNAs of seven 14-3-3 paralogs. Zygotes were flushed from the oviduct of *Tle6*^{Null} female mice (mated with normal males) at 11–13 h post human chorionic gonadotrophin injection. Scale bar, 50 μm. **l**, The average proportions of embryos on different stages in panel **k** were calculated. $N = 2$ independent experiments.

CDC25B decreased sharply in the zygotes when maternal TLE6 was depleted. A similar decrease in CDC25B was also observed in zygotes from female *Floped*^{Null} mice (Fig. 5f, h and Supplementary Figs. 14d and 15g,h). The synchronous decrease in 14-3-3 and CDC25B protein levels in SCMC-deficient oocytes and zygotes raises the possibility that the SCMC sustains CDC25B expression by stabilizing 14-3-3. Notably, 14-3-3 knockdown in zygotes reduced the protein level of CDC25B (Supplementary Fig. 11), thus supporting the speculation presented above. During late G2 phase, normal accumulation of the activity of cyclin-dependent kinase 1 (CDK1)-cyclin B (namely maturation-promoting factor, MPF) is crucial for the initiation of mitosis[47,56]. CDC25B dephosphorylates CDK1 at Tyr15 and leads to robust activation of the CDK1-cyclin B complex[18,47,57,58]. As shown in Fig. 5g, h, the expression of total CDK1 were equal between control and the zygotes from female mice lacking TLE6 or FLOPED, whereas the phosphorylation levels of CDK1 Tyr15 in the zygotes from female mice lacking TLE6 or FLOPED were significantly higher than that in control zygotes, indicating that the SCMC regulates the CDC25B-mediated dephosphorylation of CDK1 and activates MPF for timely G2/M transition in zygotes.

Increasing CDC25B activity in zygotes may somewhat rescue the blockage of early embryonic development due to SCMC dysfunction. Therefore, we injected TLE6-knockdown zygotes with wild-type *Cdc25b* mRNA or loss-of-function mutant *Cdc25b* mRNA. The developmental delay of early embryos was significantly rescued in TLE6-knockdown zygotes injected with wild-type *Cdc25b* mRNA compared with the control and TLE6-knockdown groups (Fig. 2f and Supplementary Fig. 7a,b), with the blastocyst rate increasing from 6% to 44% at 96 h pMI (Fig. 5i and Supplementary Fig. 17a). In contrast, injection of mutant *Cdc25b* mRNA did not have this effect (Fig. 5i and Supplementary Fig. 17a). Of note, the development of normal zygotes was not affected upon injection of mutant *Cdc25b* mRNA (Supplementary Fig. 7c). In addition, injection of wild-type but not mutant *Cdc25b* into TLE6-knockdown zygotes rescued the decrease in CDK1 activity caused by TLE6 deficiency, which was reflected in significantly reduced phosphorylation level of CDK1 (Supplementary Fig. 17b). Our results collectively reveal that the SCMC-14-3-3 controls CDC25B and ensures mitotic entry during the oocyte-to-embryo transition.

The human SCMC conservatively links with 14-3-3 and CDC25B

Most pathogenic mutations in human SCMC genes are associated with early embryonic cell cycle arrest[4,27]. These findings prompted us to investigate whether the SCMC-14-3-3-CDC25B cascade also exists in humans. As displayed in Fig. 6a, the human SCMC$_{core}$, which consists of MATER, TLE6, and FLOPED, interacted with 14-3-3γ in HEK-293F cells. IF staining revealed that 14-3-3 proteins in human zygotes were enriched around the subcortical region (Fig. 6b). Human TLE6 exhibited a colocalization pattern with human 14-3-3 (Fig. 6b). We then performed PLA to test the in situ association between TLE6 and 14-3-3 in human zygotes and 8-cell-stage embryo. As shown in Fig. 6c, endogenous TLE6 and 14-3-3 had definite proximate interactions in human zygotes.

Next, the possible molecular link between human SCMC and CDC25B was also determined. Co-IP assays in HEK-293F cells showed that human SCMC bound CDC25B, and this interaction was enhanced by exogenously expressed 14-3-3 (Fig. 6d). In addition, we observed subcortical colocalization between endogenous TLE6 and CDC25B in human zygotes (Fig. 6e). According to the PLA results, the TLE6 and CDC25B exhibited strong proximity signals in human GV oocytes and 2-cell-stage embryo (Fig. 6f). Overall, we demonstrate that 14-3-3 is a common component of both the mouse and human SCMC, and that it establishes a conserved molecular association between the SCMC and CDC25B.

Discussion

Malfunction of the SCMC causes dysgenesis in women, which has been well documented in clinical studies[4,27]. Predominantly accumulated in mammalian oocytes, the SCMC is indispensable for the cleavage stage of preimplantation embryos[8,9]. Despite the continual discovery of SCMC components beyond the SCMC$_{core}$ and their regulatory roles in early embryonic development[28–30], a fundamental question has not been answered at the molecular level: how does the SCMC guarantee the cleavage or cell cycle progression of preimplantation embryos?

14-3-3 is a sequence-conserved and functionally important general regulator widely present in eukaryotic cells that participates in a series of cellular processes, including the cell cycle[18,19]. Accumulating studies have revealed many client proteins that interact with and are regulated by 14-3-3[17,37]. The archetypal 14-3-3 clients are prominently represented by the CDC25 phosphatases, whose functional dynamics during cell division are tightly regulated by 14-3-3 in a phosphor-dependent manner[59,60]. Recent, two back-to-back studies have illuminated that 14-3-3 engages with the kinase pseudopodium-enriched atypical kinase (PEAK3), acting as a molecular switch that modulates PEAK3's cellular localization, scaffolding range, and interactome diversity[61,62]. Despite these efforts, the upstream regulatory factors of 14-3-3 in specific cellular contexts remain poorly understood. A recent study by Jentoft et al. discovered through mass spectrometry analysis that the content of 14-3-3 family proteins in the proteome of *Tle6*^{Null} GV oocytes was significantly decreased[31]. Consistently, our research revealed that the protein levels of 14-3-3 are protected by the SCMC during the maternal-to-embryo transition, signifying a unique mode of regulation of 14-3-3 in mammalian germ cells, although it cannot be ruled out that 14-3-3 may have feedback regulation on SCMC. In addition, studies suggested that 14-3-3 heterodimers also represent functional states[62,63]. Seven different 14-3-3 paralogs provide more significant variability in their involvement in the SCMC, which may also indicate the diversity of the functions of the SCMC. Furthermore, overexpression of 14-3-3 proteins only partially rescued the phenotype of zygotes from female *Tle6*^{Null} mice and from wild-type zygotes depleted of TLE6 (treated with Trim-Away), which indicates that stabilizing 14-3-3 is only one of the functions of the SCMC, although 14-3-3 proteins are multifunctional adapters. The other unknown binding proteins of the SCMC in mouse oocytes deserve further investigation.

https://doi.org/10.1038/s41467-024-53277-3

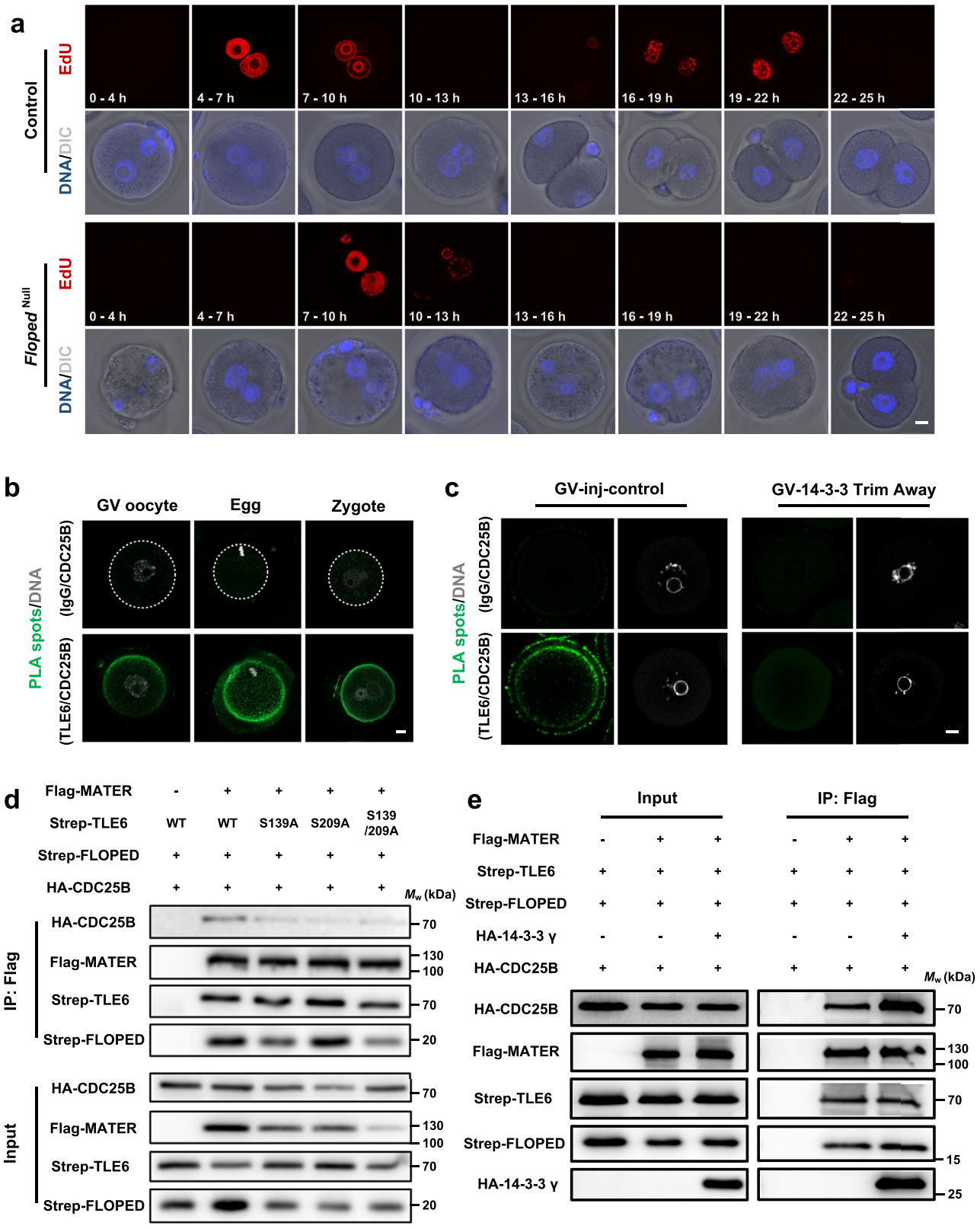

Duncan et al. reported that TLE6 is a substrate for PKA in mouse oocytes[41]. Intriguingly, predictions revealed that both TLE6 Ser139 and Ser209 are high-confidence phosphorylation sites for PKA[41], which led us to hypothesize that PKA may control the assembly of the 14-3-3-containing SCMC by phosphorylating TLE6, and the potential dynamic assembly of SCMC-14-3-3 during the development of oocytes and early embryos merits further investigation. In zygotes deficient of maternal TLE6, the addition of $TLE6_{S139/209A}$ compromises the ability of wild-type TLE6 to rescue early embryonic development, indicating that the function of the SCMC may be dependent on the proper recruitment of 14-3-3 in mammals.

The identification of 14-3-3 as a crucial structural and functional component of the SCMC provides essential molecular insight into the pleiotropic effects of the SCMC in controlling early embryonic

Fig. 4 | 14-3-3 strengthens the association between the SCMC and CDC25B. **a** Representative 5-ethynyl-2′-deoxyuridine (EdU) staining of in vitro fertilization (IVF) embryos derived from normal control and *Floped*^{Null} mouse zygotes. Mature eggs from control or *Floped*^{Null} female mice were incubated with normal sperms for 4 h and then were cultured in KSOM medium. The end of IVF were defined as time 0 h, and the presumptive fertilized eggs were treated with 10 μM EdU for denoted time intervals, fixed, permeabilized, and subjected to click reaction. Eggs used for IVF were harbored from 15 normal female mice (8 and 7 for two independent experiments) and 13 *Floped*^{Null} female mice (7 and 6 for two independent experiments). DNA was visualized with Hoechst 33342. Scale bar, 10 μm. DIC, differential interference contrast. **b** The in situ interaction between TLE6 and CDC25B in germinal vesicle (GV) oocytes, mature eggs, and zygotes from normal females were determined by proximity ligation assay (PLA) using antibodies to CDC25B and TLE6 or IgG for isotype control. DNA was visualized with DAPI. Scale bar, 10 μm. **c** Mouse GV oocytes were cultured for 5–7 h after co-microinjection with *mCherry-Trim21* mRNA + isotype IgG (for control), or *mCherry-Trim21* mRNA + anti-pan 14-3-3 antibody. The in situ interaction of TLE6 and CDC25B were determined by PLA using antibodies to CDC25B and TLE6 or IgG for isotype control. DNA was visualized with DAPI. Scale bar, 10 μm. **d** HEK-293F cells were co-transfected with expression vectors harboring Flag-tagged MATER (or a blank vector for negative control), Strep-tagged FLOPED, HA-tagged CDC25B and either Strep-tagged TLE6, $TLE6_{S139A}$ mutant, $TLE6_{S209A}$ mutant, or $TLE6_{S139/209A}$ double-site mutant as denoted. 60 h after transfection, cell lysates before (Input) or after immunoprecipitation with anti-Flag affinity agarose gel were immunoblotted as denoted. **e** HEK-293F cells were co-transfected with expression vectors as denoted. 60 h after transfection, cell lysates before (Input) or after immunoprecipitation with anti-Flag affinity agarose gel were immunoblotted for HA-tagged CDC25B, HA-tagged 14-3-3γ, Flag-tagged MATER, Strep-tagged FLOPED, and Strep-tagged TLE6.

development[9]. The dimerized 14-3-3 can simultaneously bind to two substrate proteins and thereby mediate their relationship[17]. The notable difference in binding affinity between the 14-3-3 dimer and the two phosphorylated substrate peptides of TLE6 provides extensive potential for establishing molecular connections between SCMC and other 14-3-3 clients. As a case, CDC25B probably competitively binds to one 14-3-3 protomer (14-3-3γ B) to form SCMC-14-3-3-CDC25B. According to earlier research, 14-3-3 paralogs may differentially regulate CDC25B[64]. Several studies have also revealed the specific functions of 14-3-3 paralogs in oocyte maturation[25,65,66]. It is worth investigating whether the SCMC provides multifaceted control of CDC25B during the maternal-to-embryo transition by recruiting distinct 14-3-3 paralogs. Furthermore, both the transcription and protein activity of *Cdc25b* in somatic cells are strictly controlled by complementary mechanisms to maintain the general cell cycle[46]. However, until ZGA occurs, the genomes of oocytes or embryos are silent, during which the SCMC may establish a strategy to control the functional turnover of maternal CDC25B exclusively at the protein level, through 14-3-3.

In conclusion, our study reveals that the SCMC regulates CDC25B through 14-3-3 and thus maintains the progression of the early embryonic cell cycle (Supplementary Fig. 18). In addition to their involvement in cell cycle regulation, 14-3-3 proteins also play an important role in regulating cytoskeletal organization[23,67], which seems to coincide with the role of the SCMC in controlling the symmetric division of mouse zygotes[14]. In particular, the SCMC governs the formation of the zygotic F-actin meshwork through cofilin[14]; thus, 14-3-3, a cofilin-binding protein, may also intervene in this process[67]. Moreover, the SCMC may regulate other cellular events, such as apoptosis and DNA methylation remodeling, by improving the stability of maternal proteins through 14-3-3. A recent study revealed the intrinsic involvement of the SCMC in cytoplasmic lattices, which are essential for the storage of maternal proteins in mammalian oocytes[31]. Therefore, whether 14-3-3 facilitates the configuration of cytoplasmic lattices and helps preserve proteins necessary for the development of early embryos deserves further exploration. Further investigation of 14-3-3 interacting proteins and their regulatory functions in the maternal-to-embryo transition is highly important for obtaining a comprehensive understanding of the molecular mechanisms by which the SCMC regulates early mammalian embryonic development. Moreover, these findings could lead to the development of methods for the precise diagnosis and treatment of recurrent early embryonic arrest due to mutations in SCMC genes during clinically assisted reproduction.

Methods

Collection of human oocytes and embryos

This study was approved by the Medical Research Ethics Committee of West China Second University Hospital, Sichuan University (2023 Medical scientific research for ethical approval No. 419 and 2022 Medical scientific research for ethical approval No. 291). All patients donated the samples voluntarily and signed informed consent forms.

Human GV oocytes were isolated from fresh ovarian tissues acquired from 2 females aged 32 years old with cervical adenocarcinoma during the removal of ovarian cysts. The patients had regular menstrual cycles and did not suffer from any autoimmune or genetic disorders. These patients did not undergo ovarian surgery or hormone or radiation therapy prior to ovarian cyst removal. Briefly, the fresh ovarian tissue was cut into small pieces with scissors. Oocytes were subsequently obtained by scraping away from the follicles with a 26-gauge needle in G-MOPS plus (Vitrolife, 10130) medium. Finally, the oocytes were fixed with 4% paraformaldehyde (PFA) (Beyotime, P0099) for immunofluorescence (IF) staining and proximity ligation assay (PLA).

Human embryos discarded during routine in vitro fertilization (IVF) and in vitro culture procedures were obtained. Briefly, the patients received ovarian stimulation with a gonadotropin-releasing hormone agonist/antagonist. The retrieved oocytes were then fertilized via regular IVF or intracytoplasmic sperm injection. The fertilized oocytes were cultured in G1-plus medium (Vitrolife, 10128) and transferred to G2-plus medium (Vitrolife, 10132) for blastocyst culture. The discarded embryos were fixed in 4% PFA for IF staining and PLA.

Mouse lines

All mice were maintained in compliance with the guidelines of the Animal Ethics Committee of West China Hospital, Sichuan University and the Institutional Animal Care and Use Committee (IACUC) of the Institute of Zoology, Chinese Academy of Sciences. All animal experiments were conducted in accordance with the guidelines and regulations of Sichuan University and the Institute of Zoology, Chinese Academy of Sciences. The experimental protocols were approved by the Animal Ethics Committee of West China Hospital, Sichuan University (no. 20220929004) and the IACUC of the Institute of Zoology, Chinese Academy of Sciences (no. IOZ-IACUC-2021-052 for mouse experiments).

Mice were housed in ventilated cages under a controlled 12-h light/12-h dark cycle, with ambient temperature maintained within the range of 23–25 °C and humidity levels kept within a narrow band range of 40–65%. They were provided with ad libitum access to food and water, ensuring optimal conditions for their well-being and experimental integrity. The *Floped*^{Null} mouse line was constructed using CRISPR/Cas9 gene editing technology by Beijing Viewsolid Biotech. Briefly, single guide RNAs (sgRNAs) were designed to target the ends of exon 1 and exon 3 of *Floped* (sgRNA1: AAGGTTTGCATGTCTCGCTGG, sgRNA2: TTAATGTATCCTCT CACGGGG). These sgRNAs were subsequently inserted into the eSpCas9 (1.1) plasmid. Next, Cas9/gRNA1 and Cas9/gRNA2 were coinjected into the cytoplasm of zygotes from C57BL/6 J female mice. The genotypes of the F0 mice were determined using polymerase chain reaction (PCR) with specific primers (forward primer for the wild-type allele of *Floped*: 5′- CAGACAGCAGACGAGGCACATT -3′; reverse primer for the wild-type allele of *Floped*: 5′- GTAGAGCACCAGAGGATTACTGACTTC -3′; forward primer for the gene-edited allele of *Floped*: 5′- GCTTG

https://doi.org/10.1038/s41467-024-53277-3

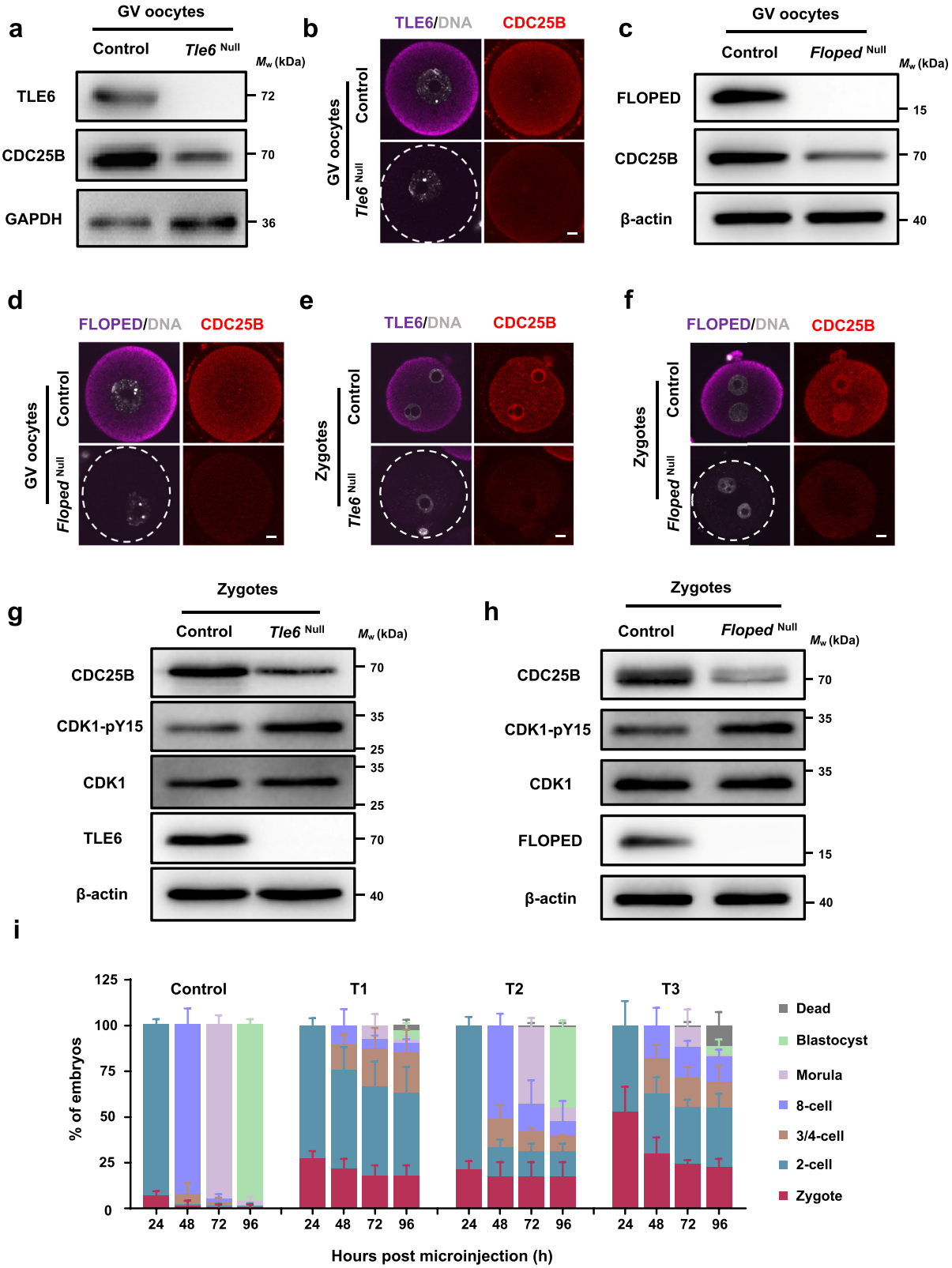

GTGTGTGCTTGTTGGTTT -3′; reverse primer for the gene-edited allele of *Floped*: 5′- CATAGCCTGTGGTCCTGAGTTTGG -3′). The F0 *Floped*$^{+/-}$ mice were crossed with wild-type C57BL/6 J mice to generate F1 heterozygotes, and F1 mice were crossed to generate F2 homozygous *Floped*^{Null} mice. *Tle6*^{Null} mice have been characterized previously[14]. All the transgenic and wild-type control mice were on the C57BL/6 J genetic background. The other mice were on the ICR genetic background.

Collection of murine oocytes and embryos

For oocyte and zygote collection, 6- to 9- week-old female mice were treated with 10 IU of pregnant mare serum gonadotropin (Nanjing Aibei Biotechnology, M2630). After 46–48 h, GV oocytes were obtained by scraping the follicles of the ovaries with a 26-gauge needle in M2 medium (Sigma-Aldrich, M7167). Mature eggs and zygotes were collected at 14–16 h (unless otherwise specified) after an additional

Fig. 5 | The SCMC-14-3-3 promotes the stability of CDC25B for mitotic entry during the maternal-to-embryo transition. a Immunoblotting of CDC25B in normal control and *Tle6*^{Null} germinal vesicle (GV) oocytes. **b** Immunofluorescence (IF) staining of CDC25B in GV oocytes isolated from control or *Tle6*^{Null} female mice. Scale bar, 10 μm. **c** Immunoblotting of CDC25B in control and *Floped*^{Null} GV oocytes. **d** IF staining of CDC25B in GV oocytes isolated from control or *Floped*^{Null} female mice. Scale bar, 10 μm. **e**, **f** IF staining of CDC25B in zygotes from control and *Tle6*^{Null} (**e**) or *Floped*^{Null} (**f**) female mice. Zygotes were flushed from the oviduct of female mice that underwent superovulation with gonadotrophins and were mated with normal males. DNA was visualized with DAPI. Scale bar, 10 μm. **g**, **h** Immunoblotting of CDC25B, CDK1, and CDK1-pY15 in zygotes from control and *Tle6*^{Null} (**g**) or *Floped*^{Null} (**h**) female mice. Zygotes were flushed from the oviduct of female mice that underwent superovulation with gonadotrophins and were mated with normal males. pY, phosphorylated tyrosine. **i**, Mouse zygotes were cultured for 24 h, 48 h, 72 h, and 96 h after co-microinjection with *mCherry-Trim21* mRNA + isotype IgG + mRNA solvent (control), *mCherry-Trim21* mRNA + anti-TLE6 antibody + mRNA solvent (T1), *mCherry-Trim21* mRNA + anti-TLE6 antibody + *Cdc25b* mRNA (T2), or *mCherry-Trim21* mRNA + anti-TLE6 antibody + $Cdc25b_{C483A/E484A}$ mRNA (T3). The proportions of embryos on different stages were calculated. $N = 3$ independent experiments. The data are presented as mean ± S.D. (standard deviation).

treatment of 5 IU human chorionic gonadotrophin (Nanjing Aibei Biotechnology, M2530) before or after mating.

Cloning

pFastBac-1 vectors encoding His-tagged mouse MATER (UniProt ID, Q9R1M5-4, 1–1059 aa), Strep-tagged mouse TLE6 (N-terminus-truncated version, 48–581 aa), Strep-tagged mouse FLOPED (1–164 aa), and Strep-tagged mouse FILIA (C-terminus-truncated versions, 1–124 aa and 1–256 aa) were described in our previous work[27]. pCAG vectors harboring Flag- and Strep-tagged mouse MATER, Strep-tagged mouse TLE6, and Strep-tagged mouse FLOPED were generated as described in our previous work[27]. pCAG vectors harboring Flag-maltose binding protein (MBP)-tagged human MATER (58–1200 aa), Strep-small ubiquitin-like modifier (SUMO)-tagged human TLE6 (146–572 aa), Strep-tagged human FLOPED, and HA-tagged human CDC25B were stored in our laboratory. The full-length coding sequences (CDSs) of seven mouse *14-3-3* and *Cdc25b* genes were amplified from mouse ovarian complementary DNA (cDNA). The full-length CDSs of all seven mouse *14-3-3* were subcloned and inserted into pGEX-6p-1. The full-length CDS of *14-3-3γ* was also subcloned and inserted into the pET-15b and pCAG vectors. The full-length CDS of mouse *Cdc25b* was subcloned and inserted into the pCAG vector with an HA tag. Other mouse *Tle6* and *Cdc25b* mutants were generated via a PCR-based strategy and subcloned and inserted into pCAG vectors.

Cell culture and transient transfection

HEK-293F cells (ThermoFisher Scientific, R79007) were maintained in SMM 293-TII Expression Medium (serum-free, complete medium, Sino Biological, M293TII). HEK-293F cells were transfected with polyethylenimine (linear, MW 25000; Polysciences, 23966). Sf9 cells (ThermoFisher Scientific, 11496015) were maintained in SIM SF Expression Medium (serum-free, Sino Biological, MSF1). To generate baculovirus, baculovirus plasmids were transfected into Sf9 cells by using Cellfectin™ II reagent (ThermoFisher Scientific, 10362100), following the manufacturer's instructions. All cells were maintained in thermostatic incubators with shaking.

Recombinant protein expression and purification

The SCMC was expressed and purified as described in a previous study[27]. Briefly, baculoviruses harboring His-tagged MATER (1–1059 aa), Strep-tagged TLE6 (48–581 aa), Strep-tagged FLOPED (1–164 aa), and Strep-tagged FILIA (1–124 aa or 1–256 aa) were used to infect Sf9 cells. After 60 h of incubation at 27 °C, the cells were collected by centrifugation at 4 °C and 800 × *g* for 15 min, suspended in lysis buffer containing 25 mM Tris, 150 mM NaCl, 1 mM phenylmethylsulfonyl fluoride (PMSF; VWR Chemicals, P105539), 0.8 μM aprotinin (Sangon Biotech, A600153), 2 μM pepstatin A (Sangon Biotech, A610583), and 5 μg/mL leupeptin (Sangon Biotech, A600580) (pH 8.0), and lysed with a high-pressure cell disrupter at 6 °C. The cell debris was removed by centrifugation at 4 °C and 27000 × *g* for 30 min, and the supernatant was incubated with Ni-NTA (Qiagen, 30250). The resin was washed with lysis buffer containing 30 mM imidazole (Sigma–Aldrich, 288-32-4) and the protein was eluted with lysis buffer containing 300 mM imidazole. The eluted proteins were subjected to ion-exchange chromatography (IEC, SOURCE™ 15Q, GE Healthcare, 17094705) with buffer A, which contained 25 mM Tris and 5 mM dithiothreitol (DTT; INALCO, 1758-9030) (pH 8.0), and buffer B, which contained 25 mM Tris, 800 mM NaCl, and 5 mM DTT (pH 8.0). The collective fractions corresponding to the same peak were subjected to size-exclusion chromatography (Superose™ 6 Increase 10/300 GL; GE Healthcare, 29091596) for further purification, and subjected to sodium dodecyl sulfate-polyacrylamide gel electrophoresis (SDS-PAGE). The gel strips of additional proteins derived from the IEC peak representing a more negative charge were analyzed by mass spectrometry. The two bands of proteins were verified to be endogenous 14-3-3 proteins in Sf9 cells. The fractions corresponding to the other peak without endogenous 14-3-3 proteins were used for reconstituting the mouse 14-3-3-containing SCMC. The expression and purification of $SCMC_{core}$, including His-tagged MATER (1–1059 aa), Strep-tagged TLE6 (48–581 aa), and Strep-tagged FLOPED (1–164 aa), were performed by the same procedure as described above.

For the expression of glutathione S-transferase (GST)-tagged 14-3-3 proteins, *Escherichia coli* (*E. coli*) BL21(DE3) (ThermoFisher Scientific, EC0114) was transformed with individual pGEX-6p-1 vectors harboring each 14-3-3 paralog and stimulated overnight with 200 μM isopropyl β-D-thiogalactoside (BLUEPUS, 3001858) at 20 °C. The cells were collected by centrifugation at 4 °C and 4000 × *g* for 15 min, suspended in lysis buffer containing 1 mM PMSF, and lysed with a high-pressure cell disrupter at 6 °C. The cell debris was removed by centrifugation at 4 °C and 27000 × *g* for 30 min, and the supernatant was incubated with Glutathione Sepharose 4B (GE Healthcare, 17075601) for 1 h. The resin was washed with lysis buffer and eluted with lysis buffer containing 15 mM reduced glutathione (pH 8.0). The GST-tag on the 14-3-3 proteins was removed by incubation with 3 C protease overnight, after which the samples were further purified with SOURCE 15Q as described above, and the fractions corresponding to the same peak were collected and subjected to size-exclusion chromatography (Superdex™ 200 Increase 10/300 GL; GE Healthcare, 28990944) for further purification.

Pull-down and co-immunoprecipitation (co-IP)

For pull-down assays, SCMC proteins (with Strep-tagged TLE6, FLOPED, and/or FILIA) and mouse 14-3-3 paralogs were purified from Sf9 cells and *E. coli*, respectively, as described above. Lysates of normal eggs or 14-3-3 proteins were incubated with the SCMC or an equal volume of buffer (as a negative control). The samples were then incubated with Strep-Tactin resin (IBA Life Sciences, 2-4030-025) at 4 °C, and the resin was subjected to extensive rinsing with washing buffer containing 0.5% Nonidet P-40 (NP-40, Sangon Biotech, A600385-0100). Proteins bound to the resin were eluted using elution buffer containing 50 mM biotin, and the pull-down products were further analyzed by SDS-PAGE and/or immunoblotting.

For co-IP assays, lysates from normal eggs (1000) were precipitated with Pierce™ Protein A/G Magnetic Beads (ThermoFisher Scientific, 88802) by using anti-MATER, anti-TLE6, or anti-FLOPED antibodies. Isotype immunoglobulin G (IgG) was used as a negative control: guinea pig IgG (H + L) (Sangon Biotech, D110505), rabbit IgG

https://doi.org/10.1038/s41467-024-53277-3

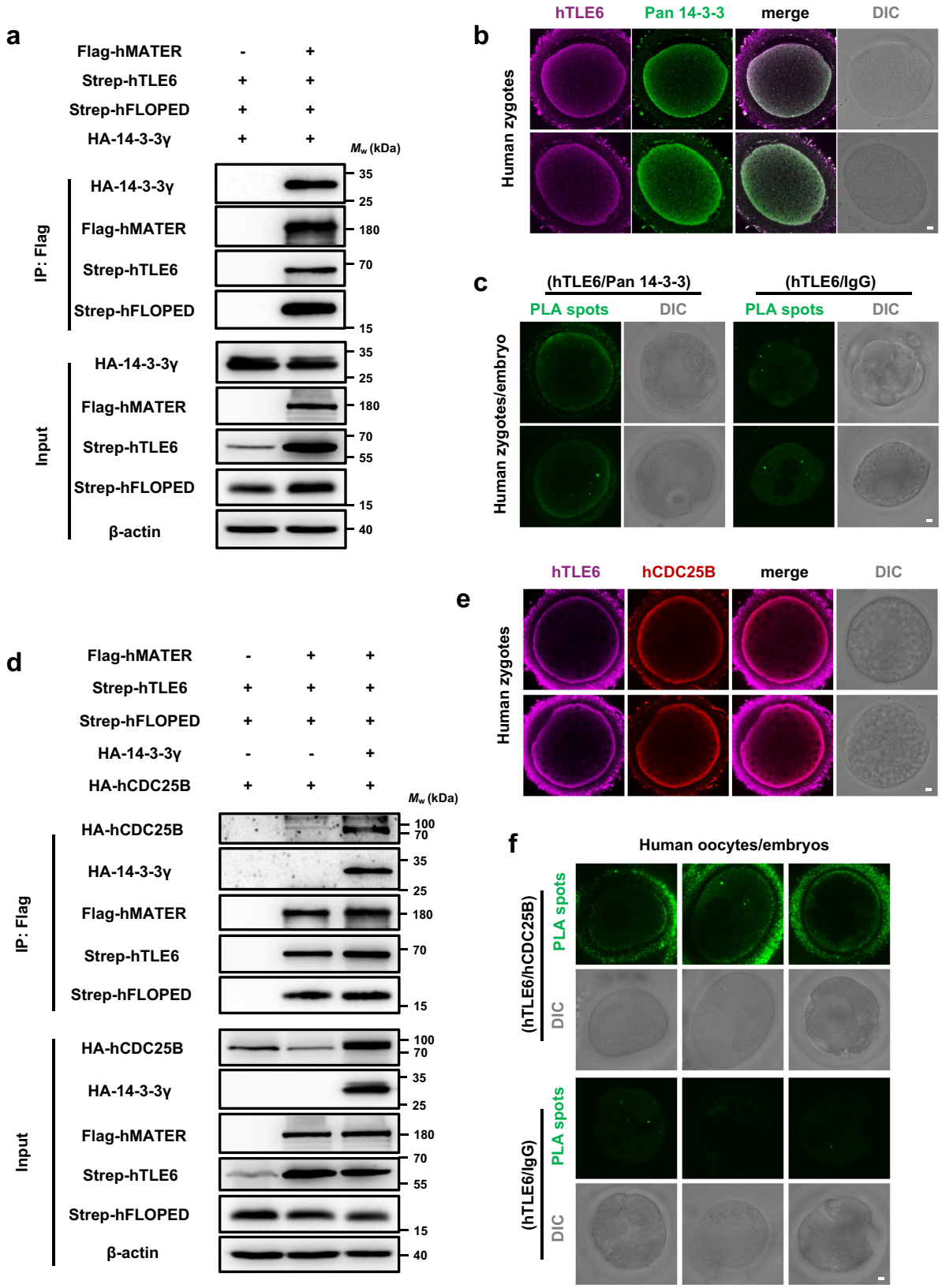

(Beyotime, A7016), and mouse IgG (Beyotime, A7028). In addition, pCAG expression vectors harboring SCMC subunits, 14-3-3γ and/or CDC25B were cotransfected into HEK-293F cells as described above. Cell groups that were not transfected with the bait protein were used as negative controls. Sixty hours after transfection, the cells were collected and washed with phosphate buffered saline (PBS; Solarbio, P1000). Cell extracts were lysed in lysis buffer containing 1% NP-40 and clarified via centrifugation. Then, the protein extracts were precipitated with ANTI-FLAG® M2 Affinity Gel at 4 °C. After washing in lysis buffer, the proteins were eluted with elution buffer containing 0.4 mg/mL flag peptide. The co-IP products were further analyzed by immunoblotting.

Fig. 6 | The human SCMC interacts with 14-3-3 and establishes conserved molecular association with CDC25B. a HEK-293F cells were co-transfected with expression vectors harboring Flag-MBP-tagged hMATER (or a blank vector for negative control), Strep-SUMO-tagged hTLE6, Strep-tagged hFLOPED, and HA-tagged 14-3-3γ. 60 h after transfection, cell lysates before (Input) or after immunoprecipitation with anti-Flag affinity agarose gel were immunoblotted for HA-tagged 14-3-3γ, Flag-MBP-tagged hMATER, Strep-SUMO-tagged hTLE6, and Strep-tagged hFLOPED. hMATER, human MATER. hTLE6, human TLE6. hFLOPED, human FLOPED. **b** Human zygotes were fixed, permeabilized, and incubated with antibodies to TLE6 and pan 14-3-3. The zygotes were imaged by confocal and differential interference contrast (DIC) microscopy. Scale bar, 10 μm. Colocalization of hTLE6 and pan 14-3-3 was presented in the merge. **c** The in situ interaction between hTLE6 and pan 14-3-3 in human zygotes and 8-cell-stage embryo was determined by proximity ligation assay (PLA) using antibodies to TLE6 and pan 14-3-3 or IgG for isotype control. Scale bar, 10 μm. **d** HEK-293F cells were co-transfected with expression vectors harboring Flag-MBP-tagged hMATER (or a blank vector for negative control), Strep-SUMO-tagged hTLE6, Strep-tagged hFLOPED, HA-tagged hCDC25B, and either HA-tagged 14-3-3γ or blank vector as denoted. 60 h after transfection, cell lysates before (Input) or after immunoprecipitation with anti-Flag affinity agarose gel were immunoblotted for HA-tagged hCDC25B, HA-tagged 14-3-3γ, Flag-MBP-tagged hMATER, Strep-SUMO-tagged hTLE6, and Strep-tagged hFLOPED. hCDC25B, human CDC25B. **e** Human zygotes were fixed, permeabilized, and incubated with antibodies to TLE6 and CDC25B. The zygotes were imaged by confocal and DIC microscopy. Scale bar, 10 μm. Colocalization of hTLE6 and hCDC25B was presented in the merge. **f** The in situ interaction between hTLE6 and hCDC25B in human GV oocytes and embryos was determined by PLA using antibodies to TLE6 and CDC25B or IgG for isotype control. Scale bar, 10 μm.

Immunoblotting

Samples for immunoblotting were prepared with SDS sample buffer containing 20 mM DTT, separated via SDS-PAGE and subsequently transferred to polyvinylidene difluoride membranes (Millipore). The membranes were blocked in Tris-buffered saline containing 0.1% Tween-20 (Sigma-Aldrich, 9005-64-5) and 5% nonfat milk powder (TBST) and subsequently incubated with primary antibodies at 4 °C overnight. After being subjected to extensive rinsing with TBST, the membranes were incubated with horseradish peroxidase (HRP)-conjugated secondary antibodies at room temperature. The membranes were then rinsed in TBST, and immunoreactivity was detected with a supersensitive ECL chemiluminescent substrate (Biosharp, BL520B). Images of the blots were acquired by using G:BOX Chemi XRQ (Syngene). The primary antibodies used were as follows: rabbit anti-14-3-3 (pan) antibody (Cell Signaling Technology, 8312, lot 4), rabbit anti-14-3-3 pan polyclonal antibody (ThermoFisher Scientific, 51-0700, lot XK366865), mouse anti-NLRP5 antibody (Novus Biologicals, NBP1-76289, lot 5959-2004), anti-FLOPED antibody[8], mouse anti-TLE6 antibody (Abmart, M034864, lot 10042800), rabbit anti-TLE6 antibody (Abmart, PU440858, lot 10179035), mouse anti-CDC25B monoclonal antibody (Proteintech, 67145-1-Ig, lot 10009433), rabbit anti-CDK1-Specific polyclonal antibody (Proteintech, 19532-1-AP, lot 00109786), rabbit anti-phospho-cdc2 (Tyr15) antibody (Cell Signaling Technology, 9111S, lot 12), rabbit anti-GAPDH antibody (Abcam, ab181602, lot 3523022348), rabbit anti-DDDDK-Tag mAb (ABclonal, AE063, lot 9100026002), rabbit anti-HA-tag pAb (ABclonal, AE036), mouse anti-strep-tag monoclonal antibody (Huaxingbio, HX1816, lot 620s320316), and HRP-conjugated rabbit anti-β-Actin mAb (ABclonal, AC028, lot 3522070661). The secondary antibodies used were as follows: HRP-conjugated goat anti-guinea pig IgG (H + L) (ABclonal, AS025), goat anti-mouse IgG H&L (HRP) (ZenBio, 511103), and goat anti-rabbit IgG H&L (HRP) (ZenBio, 511203).

In vitro fertilization (IVF)

IVF was conducted as previously described[68]. Briefly, sperm were collected from the caudal epididymides of male C57BL/6 J mice aged 7 to 12 weeks and capacitated in modified Krebs-Ringer bicarbonate medium (TYH; Nanjing Aibei Biotechnology, M2030) at 37 °C in a 5% CO_2 incubator. Mature eggs were washed in human tubal fluid medium (HTF; Nanjing Aibei Biotechnology, M1130) and then incubated with sperm after capacitation for 4–6 hours in HTF medium in humidified 5% CO_2 in air at 37 °C. The presumptive fertilized eggs were washed with KSOM (Nanjing Aibei Biotechnology, M1430) medium three times and cultured in KSOM medium for analysis.

Immunofluorescence (IF) staining and confocal microscopy

Oocytes and embryos were fixed with 2% PFA at 37 °C for 30 min followed by permeabilization in 0.5% Triton X-100 (Sigma–Aldrich, 9036-19-5) overnight at 4 °C after washing with PBST (PBS containing 0.1% Triton X-100). The samples were blocked with 3% BSA (Biofroxx, 4240GR025) for 5 h at room temperature (RT), and then incubated with primary antibodies overnight at 4 °C. The embryos were washed three times in PBST and incubated with specific fluorophore-conjugated secondary antibodies for 1 h at RT. After washing in PBST three times, the samples were stained with DAPI (Beyotime, C1006), and images were taken with a Zeiss LSM 980 (Carl Zeiss) and an Olympus FLUOVIEW FV3000. The primary antibodies used were as follows: rabbit anti-14-3-3 pan polyclonal antibody (ThermoFisher Scientific, 51-0700, lot XK366865), mouse anti-NLRP5 antibody (Novus Biologicals, NBP1-76289, lot 5959-2004), anti-FLOPED antibody[8], mouse anti-TLE6 antibody (Abmart, M034864, lot 10042800), rabbit anti-TLE6 antibody (Abmart, PU440858, lot 10179035), mouse anti-CDC25B monoclonal antibody (Proteintech, 67145-1-Ig, lot 10009433), rabbit Cdc25B Polyclonal Antibody (ThermoFisher Scientific, PA5-17759, lot ZD4309764), and rabbit anti-phospho-CDK1 (Tyr15) polyclonal antibody (Beyotime, AF5761, lot 091223240529). The secondary antibodies used were Alexa Fluor® 488-AffiniPure goat anti-mouse IgG (H + L) (Jackson ImmunoResearch, 115-545-062, lot 152087) and Rhodamine Red-X-AffiniPure Goat Anti-Rabbit IgG (H + L) (Jackson ImmunoResearch, 111-295-144, lot 91274). The mouse anti-NLRP5 antibody (Novus Biologicals, NBP1-76289), anti-FLOPED antibody[8], and rabbit TLE6 antibody (Abmart, PU440858) were conjugated to Alexa Fluor® 647 using the Apex™ Alexa Fluor™ 647 Antibody Labeling Kit following the manufacturer's instructions (ThermoFisher Scientific, 10359016). The mouse anti-CDC25B monoclonal antibody (Proteintech, 67145-1-Ig) and Cdc25B Polyclonal Antibody (ThermoFisher Scientific, PA5-17759) were conjugated to Alexa Fluor™ 488 using Alexa Fluor® 488 Antibody Labeling Kit following the manufacturer's instructions (ThermoFisher Scientific, A20181).

Cryo-electron microscopy sample preparation and data collection

The purified SCMC-14-3-3γ was thawed, applied to glow-discharged 200-mesh alloy grids (Quantifoil Au200, R1.2/1.3) and subsequently vitrified using Vitrobot Mark IV. The movie stacks were collected in counted-Nanoprobe mode on a 300 kV Titan Krios Gi3 electron microscope (ThermoFisher Scientific) equipped with a Gatan K3 Summit detector and a GIF Quantum energy filter. All movie stacks with 50 frames were collected using SerialEM software at a nominal magnification of 105,000×, a pixel size of 0.85 Å, and a defocus range from −1.2 μm to −1.8 μm. Each movie stack was for 3.5 s in length with 0.07 s of exposure per frame, for a total dose of 56.15 e-/Å^2.

Single-particle data analysis

A total of 2218 movies were collected and processed in RELION 3.1[69]. After correction of the beam-induced motion by MotionCor2[70], contrast transfer function parameters were estimated by Gctf[71]. A total of 1917346 particles were autopicked using the LOG method and extracted at a pixel size of 1.70 Å. A reference map was generated after one round of 2D classification, initial model generation, and one round

of 3D classification. Using the map as a 3D reference for autopicking, 1441737 particles were picked and extracted at a pixel size of 1.70 Å. A total of 366691 particles were screened out after one round of 3D classification. The selected particles were re-extracted at an original pixel size of 0.85 Å, and one round of 3D classification without alignment was performed with a mask on the complex. A total of 41406 particles were finally subjected to 3D refinement after CTF refinement and particle polishing, yielding a density map with a 3.0 Å resolution.

Model building and refinement

The initial model of the SCMC-14-3-3γ was generated by rigid docking of the $SCMC_{core}$ structure (Protein Data Bank, PDB: 8H96) and the 14-3-3γ homodimer structure (PDB: 2B05) into the cryo-EM map using ChimeraX[72]. The model was further refined using real-space refinement tool of PHENIX[73] and manually adjusted using COOT[74]. After refinement, additional densities were observed within the highly conserved binding pockets of 14-3-3γ.

For the identification of phosphopeptide TLE6 (133–144) pS139, the main chain was de novo built by referencing the unsharpened map to ensure clear continuity with surrounding residues. In addition, phosphorylation of Ser139 was identified by mass spectrometry analysis.

For the building of phosphopeptide TLE6 (203–214) pS209, initial model building was challenging due to the discontinuity of this density in this region. To accurately build the model, a combined approach utilizing in silico prediction by 14-3-3-Pred (https://www.compbio.dundee.ac.uk/1433pred/), co-IP, isothermal titration calorimetry (ITC), and mass spectrometry analysis was employed. In addition, previous study showed that PKA-mediated phosphorylation of TLE6 is essential for mouse oocyte maturation[41], and phosphorylation of Ser209 on TLE6 was well confirmed by mass spectrometry analysis.

Following the phosphorylated peptides identification and model adjustments, the final stages of real-space refinement were performed in PHENIX[73] using a B-factor sharpened map. The cryo-EM maps and the refined atomic coordinates of the SCMC-14-3-3γ complex have been deposited in the Electron Microscopy Data Bank (EMDB: EMD-38369) and the Protein Data Bank (PDB: 8XI3), respectively. Statistics for data collection and structural refinement are shown in Supplementary Table 1. The illustrated figures were generated using ChimeraX[72].

Mass spectrometry (MS) analysis

To identify the copurified proteins in the SCMC, the samples were subjected to SDS-PAGE, and two additional protein bands were excised. The excised gel strip samples underwent reduction, alkylation, and enzymatic digestion, followed by desalination. Subsequent to these procedures, samples were analyzed through the Q Exactive Plus mass spectrometer. The raw mass spectrometry files of the proteome were searched using Maxquant (v1.6.2.3), referring to the *Spodoptera frugiperda* database (updated in May 2021; 28,456 sequences). Precursor ions were allowed a mass deviation of up to 10 ppm, while fragment ions were limited to a mass deviation of 0.02 Da. The maximum allowable count of missed cleavage sites was set at 2. Fixed modifications included cysteine carbamido methylation and methionine oxidation. Both peptide and protein false discovery rates were maintained below 1%. Peptides were required to consist of at least 6 amino acids, with a maximum peptide molecular weight of 12,000 Da.

To identify the phosphorylation of the SCMC, 50 μg of the protein solution underwent reduction and alkylation. The protein solution was precipitated using a methanol/chloroform/water mixture, and the resulting precipitate was dissolved in 50 mM triethylammonium bicarbonate (Sigma), followed by enzymatic digestion and desalination. Desalted peptides were analyzed by an EASY-nanoLC 1200 system coupled with a Q Exactive HF-X mass spectrometer. The flow rate of the analytical column was 330 nl/min with a 65 min gradient from 8% to 100% buffer B (80% ACN and 0.1% formic acid). For the full MS scans, ions with m/z ranging from 350 to 1800 were acquired under data-dependent acquisition mode by orbitrap with a resolution of 30,000 at m/z = 200. For the MS2 scans, the top 20 most intense parent ions were selected with an isolation window of 1.6 m/z and fragmented with stepped NCE values of 25% and 27%. The proteomics data were searched against the mouse protein sequence database (updated in July 2019; 17,019 sequences). The proteolytic enzyme was trypsin, or α-Lytic Protease and two missed cleavage sites were allowed. Oxidation of methionine and acetylation of the protein N terminus were set as variable modifications. Cysteine carbamidomethylation was set as a fixed modification. Phosphorylation at S, T, or Y residues was also set as a variable modification. The maximum peptide mass was set to 5000 Da, and the minimum amino acid length was set to 6. The precursor mass tolerance was set to 10 ppm, and the fragment mass tolerance was set at 0.02 Da.

Isothermal titration calorimetry (ITC)

The binding affinity between 14-3-3γ and wild-type TLE6 peptides (TLE6 (133–144) or TLE6 (203–214)) or modified peptides carrying phosphorylated TLE6 Ser139/209/223 (TLE6 (133–144) pS139, TLE6 (203–214) pS209, or TLE6 (217–228) pS223) was measured using a MicroCal ITC200 instrument (Malvern) at 25 °C. His-tagged 14-3-3γ was prepared in buffer containing 25 mM HEPES and 150 mM NaCl (pH 7.5). All TLE6 peptides were dissolved in the same buffer mentioned above. TLE6 (133–144) or TLE6 (133–144) pS139 (1.3 mM) was titrated into 50 μM 14-3-3γ protein. TLE6 (203–214) or TLE6 (203–214) pS209 (2.5 mM) was titrated into 70 μM 14-3-3γ protein. TLE6 (217–228) pS223 (1.3 mM) was titrated into 50 μM 14-3-3γ protein. The data were normalized by dilution heat, and processed with PEAQ-ITC Origin software (MicroCal) for curve fitting and determination of the equilibrium dissociation constant (K_d). All titrations were repeated three times. The data represented mean ± S.D. (standard deviation) of 3 independent experiments.

In vitro transcription and microinjection of oocytes and zygotes

The CDSs of *Trim21*, *Tle6*, seven *14-3-3* paralogs, and *Cdc25b* were inserted into the Pcs2 vector and transcribed according to the instructions of the SP6 message mMACHINE Kit (ThermoFisher Scientific, AM1340). The in vitro-transcribed mRNAs were resuspended in nuclease-free water via the lithium chloride precipitation method. For GV oocyte microinjection, GV oocytes were incubated in M2 medium supplemented with 0.2 mM isobutylmethylxanthine (GLPBIO, GC11730) to inhibit spontaneous germinal vesicle breakdown.

For Trim-Away assays, *Trim21* mRNA mixed with an anti-TLE6 (Abmart, M034864) or anti-pan 14-3-3 antibody (Cell Signaling Technology, 8312) was injected into mouse GV oocytes or zygotes before the PN2 stage, and comicroinjection of *Trim21* mRNA and isotype IgG (ZenBio, 511103) was used as a control. Then, the GV oocytes or embryos were cultured in IVM (Nanjing Aibei Biotechnology, M2115) or KSOM, respectively, for the following analysis. For mRNA supplementation, mixed mRNAs encoding seven 14-3-3 paralogs were microinjected into zygotes from female $Tle6^{Null}$ mice. For the combination of Trim-Away and mRNA supplementation, when the zygotes were treated with Trim-Away, they were simultaneously injected with mRNAs encoding TLE6, seven 14-3-3 paralogs, or CDC25B. After microinjection, the zygotes were cultured in KSOM for the following analysis.

Inhibitor treatment

To block PKA, zygotes were collected and cultured in KSOM medium containing 20 μM H89 (Selleck, S1582). Zygotes cultured in KSOM medium with DMSO were used as control.

Proximity ligation assay (PLA)

The PLA was performed using Duolink® PLA Fluorescence (rabbit Plus probe DUO92002, mouse Minus probe DUO92004, detection reagents DUO92014, washing buffer DUO82049) according to the manufacturer's protocol (Sigma-Aldrich). The steps prior to detection of the PLA probes were the same as that used for IF staining. The oocytes and zygotes were collected and fixed with 4% PFA for 30 min at RT. Then, the samples were permeabilized with 0.5% Triton X-100 in PBS for 30 min at RT and blocked with Duolink® Blocking Solution for 60 min at 37 °C in a humidified chamber. The embryos were incubated with primary antibodies in Duolink® Antibody Diluent at 4 °C overnight, and washed with PBSA (PBS containing 0.1% BSA) the next day. Subsequently, the samples were transferred to the probe mixture in a 37 °C-humidity chamber for 1 h. After washing step with 1×Duolink® washing buffer A, ligation attached to the PLA probes was performed for 30 min at 37°C, followed by amplification for 100 min at 37°C in the dark. After a series of washes with 1×Duolink® washing buffer B and 0.01×Duolink® washing buffer B, the embryos were counterstained with DAPI and imaged with a Zeiss LSM980 (Carl Zeiss) or Olympus FLUOVIEW FV3000 microscope.

RNA isolation and quantitative real-time PCR (qRT-PCR)

As described previously[75,76], oocytes (30 oocytes per sample) were transferred to 12.6 µl of lysis buffer, containing 0.2% Triton X-100, dNTPs (TIANGEN, CD111-03), oligo-dT primers and an RNase inhibitor (Sangon Biotech, B600478) and lysed at 72 °C for 30 min. cDNA was synthesized according to the manufacturer's instructions using EasyScript® One-Step gDNA Removal and cDNA Synthesis SuperMix (Transgene, AE311-03). RT-qPCR was carried out with ChamQ SYBR® qPCR Master Mix (Vazyme, Q311-02) and a CFX Connect™ Real-Time PCR Detection System (Bio-Rad). The sequences of the primers for mouse *Cdc25b* and *Gapdh* were as follows: *Cdc25b* (GenBank Accession, NM_023117.4 and NM_001111075.4), forward primer: 5′-GTGATCCGACCCATCCTCAAG-3′ and reverse primer: 5′-TGTTTGCCATCCACGGTCTG-3′; *Gapdh* (GenBank Accession, NM_001289726.2), forward primer: 5′-GTGTTCCTACCCCCAATGTGT-3′ and reverse primer: 5′-ATTGTCATACCAGGAAATGAGCTT-3′. The primers for the seven mouse 14-3-3 paralogs were designed as previously described[25]. Relative mRNA levels were normalized to endogenous *Gapdh* mRNA levels, and the experiment was repeated for four independently obtained samples.

Measurement of DNA synthesis in embryos

DNA synthesis in 1-cell embryos was measured via 5-ethynyl-2′-deoxyuridine (EdU) staining using a BeyoClick™ EdU Cell Proliferation Kit with Alexa Fluor 488 (Beyotime, C0071). Briefly, mature eggs were incubated with sperm for 4 h according to the IVF protocol. Here, we defined the end of IVF as hour 0. The presumptive fertilized eggs were treated with 10 µM EdU at 37 °C in a 5% CO_2 incubator for the indicated intervals and then fixed in 4% PFA for 30 min, followed by permeabilization in 0.5% Triton X-100 for 30 min at RT. After being washed with PBST, the embryos were transferred to click reaction solution and incubated for 30 min in the dark at RT. Next, the embryos were counterstained with Hoechst 33342 for 30 min and finally viewed with an Olympus FLUOVIEW FV3000.

Statistics and reproducibility

For quantitative analyzes, at least three replicates were performed, and the data are expressed as the mean ± S.D. GraphPad Prism (GraphPad Software, Inc., La Jolla, CA, USA) was used to carry out statistical analysis, and analysis of variance (ANOVA) or a two-tailed unpaired Student's *t*-test was used to compare differences between two groups. Statistical significance is indicated as follows: $^{*}P < 0.05$, $^{**}P < 0.01$, and $^{***}P < 0.001$; *ns* indicates $P > 0.05$. The IF staining and immunoblotting assays were performed at least two or three independent repetitions with similar results.

Reporting summary

Further information on research design is available in the Nature Portfolio Reporting Summary linked to this article.

Data availability

All data generated or analyzed in this study are included in the paper and its Supplementary information files. The cryo-EM density map and corresponding atomic coordinate have been deposited in the Electron Microscopy Data Bank under accession code EMD-38369 and the Protein Data Bank (PDB) under accession number 8XI3, respectively. Initial models used for model building were PDB ID codes 8H96 and 2B05. The mass spectrometry data have been deposited to the ProteomeXchange Consortium via the iProX[77,78] partner repository with the dataset identifier PXD055498. Source data are provided with this paper.

References

1. Tong, Z. B. et al. Mater, a maternal effect gene required for early embryonic development in mice. *Nat. Genet* **26**, 267–268 (2000).
2. Christians, E., Davis, A. A., Thomas, S. D. & Benjamin, I. J. Maternal effect of Hsf1 on reproductive success. *Nature* **407**, 693–694 (2000).
3. Innocenti, F. et al. Maternal effect factors that contribute to oocytes developmental competence: an update. *J. Assist Reprod. Gen.* **39**, 861–871 (2022).
4. Mitchell, L. E. Maternal effect genes: Update and review of evidence for a link with birth defects. *HGG Adv.* **3**, 100067 (2022).
5. Wu, D. & Dean, J. Maternal factors regulating preimplantation development in mice. *Curr. Top. Dev. Biol.* **140**, 317–340 (2020).
6. Li, L., Zheng, P. & Dean, J. Maternal control of early mouse development. *Development* **137**, 859–870 (2010).
7. Eckersley-Maslin, M. A., Alda-Catalinas, C. & Reik, W. Dynamics of the epigenetic landscape during the maternal-to-zygotic transition. *Nat. Rev. Mol. Cell Biol.* **19**, 436–450 (2018).
8. Li, L., Baibakov, B. & Dean, J. A subcortical maternal complex essential for preimplantation mouse embryogenesis. *Dev. Cell* **15**, 416–425 (2008).
9. Lu, X., Gao, Z., Qin, D. & Li, L. A maternal functional module in the mammalian oocyte-to-embryo transition. *Trends Mol. Med* **23**, 1014–1023 (2017).
10. Zhu, K. et al. Identification of a human subcortical maternal complex. *Mol. Hum. Reprod.* **21**, 320–329 (2015).
11. Tong, X. M. et al. Mutations in OOEP and NLRP5 identified in infertile patients with early embryonic arrest. *Hum. Mutat.* **43**, 1909–1920 (2022).
12. Mu, J. et al. Mutations in NLRP2 and NLRP5 cause female infertility characterised by early embryonic arrest. *J. Med Genet* **56**, 471–480 (2019).
13. Zheng, W. et al. Expanding the genetic and phenotypic spectrum of the subcortical maternal complex genes in recurrent preimplantation embryonic arrest. *Clin. Genet* **99**, 286–291 (2021).
14. Yu, X. J. et al. The subcortical maternal complex controls symmetric division of mouse zygotes by regulating F-actin dynamics. *Nat. Commun.* **5**, 4887 (2014).
15. Tzivion, G., Shen, Y. H. & Zhu, J. 14-3-3 proteins; bringing new definitions to scaffolding. *Oncogene* **20**, 6331–6338 (2001).
16. Hermeking, H. The 14-3-3 cancer connection. *Nat. Rev. Cancer* **3**, 931–943 (2003).
17. Fu, H., Subramanian, R. R. & Masters, S. C. 14-3-3 proteins: structure, function, and regulation. *Annu Rev. Pharm. Toxicol.* **40**, 617–647 (2000).
18. Reinhardt, H. C. & Yaffe, M. B. Phospho-Ser/Thr-binding domains: navigating the cell cycle and DNA damage response. *Nat. Rev. Mol. Cell Biol.* **14**, 563–580 (2013).
19. Hermeking, H. & Benzinger, A. 14-3-3 proteins in cell cycle regulation. *Semin Cancer Biol.* **16**, 183–192 (2006).

20. Pennington, K. L., Chan, T. Y., Torres, M. P. & Andersen, J. L. The dynamic and stress-adaptive signaling hub of 14-3-3: emerging mechanisms of regulation and context-dependent protein-protein interactions. *Oncogene* **37**, 5587–5604 (2018).
21. Zha, J., Harada, H., Yang, E., Jockel, J. & Korsmeyer, S. J. Serine phosphorylation of death agonist BAD in response to survival factor results in binding to 14-3-3 not BCL-X(L). *Cell* **87**, 619–628 (1996).
22. Schlegelmilch, K. et al. Yap1 acts downstream of alpha-catenin to control epidermal proliferation. *Cell* **144**, 782–795 (2011).
23. Moreno-Vicente, R. et al. Caveolin-1 modulates mechanotransduction responses to substrate stiffness through actin-dependent control of YAP. *Cell Rep.* **25**, 1622–1635.e1626 (2018).
24. Aghazadeh, Y. & Papadopoulos, V. The role of the 14-3-3 protein family in health, disease, and drug development. *Drug Discov. Today* **21**, 278–287 (2016).
25. Eisa, A. A. et al. YWHA (14-3-3) protein isoforms and their interactions with CDC25B phosphatase in mouse oogenesis and oocyte maturation. *BMC Dev. Biol.* **19**, 20 (2019).
26. Cui, C. et al. 14-3-3 epsilon prevents G2/M transition of fertilized mouse eggs by binding with CDC25B. *BMC Dev. Biol.* **14**, 33 (2014).
27. Chi, P. et al. Structural basis of the subcortical maternal complex and its implications in reproductive disorders. *Nat. Struct. Mol. Biol.* **31**, 115–124 (2024).
28. Qin, D. et al. The subcortical maternal complex protein Nlrp4f is involved in cytoplasmic lattice formation and organelle distribution. *Development* **146**, dev183616 (2019).
29. Mahadevan, S. et al. Maternally expressed NLRP2 links the subcortical maternal complex (SCMC) to fertility, embryogenesis and epigenetic reprogramming. *Sci. Rep.* **7**, 44667 (2017).
30. Gao, Z. et al. Zbed3 participates in the subcortical maternal complex and regulates the distribution of organelles. *J. Mol. Cell Biol.* **10**, 74–88 (2018).
31. Jentoft, I. M. A. et al. Mammalian oocytes store proteins for the early embryo on cytoplasmic lattices. *Cell* **186**, 5308–5327.e5325 (2023).
32. De, S., Marcinkiewicz, J. L., Vijayaraghavan, S. & Kline, D. Expression of 14-3-3 protein isoforms in mouse oocytes, eggs and ovarian follicular development. *BMC Res Notes* **5**, 57 (2012).
33. Zhang, H. M. et al. Stable maternal proteins underlie distinct transcriptome, translatome, and proteome reprogramming during mouse oocyte-to-embryo transition. *Genome Biol.* **24**, 166 (2023).
34. Sun, H. Z. et al. Proteomic profiling reveals the molecular control of maturation. *Mol. Cell Proteom.* **22**, 100481 (2023).
35. Xiao, B. et al. Structure of a 14-3-3 protein and implications for coordination of multiple signalling pathways. *Nature* **376**, 188–191 (1995).
36. Liu, D. et al. Crystal structure of the zeta isoform of the 14-3-3 protein. *Nature* **376**, 191–194 (1995).
37. Segal, D. et al. A central chaperone-like role for 14-3-3 proteins in human cells. *Mol. Cell* **83**, 974–993.e915 (2023).
38. Obsil, T., Ghirlando, R., Klein, D. C., Ganguly, S. & Dyda, F. Crystal structure of the 14-3-3zeta:serotonin N-acetyltransferase complex. a role for scaffolding in enzyme regulation. *Cell* **105**, 257–267 (2001).
39. Stevers, L. M. et al. Characterization and small- molecule stabilization of the multisite tandem binding between 14-3-3 and the R domain of CFTR. *P Natl Acad. Sci. USA* **113**, E1152–E1161 (2016).
40. Madeira, F. et al. 14-3-3-Pred: improved methods to predict 14-3-3-binding phosphopeptides. *Bioinformatics* **31**, 2276–2283 (2015).
41. Duncan, F. E. et al. Transducin-like enhancer of split-6 (TLE6) is a substrate of protein kinase a activity during mouse oocyte maturation. *Biol. Reprod.* **90**, 63 (2014).
42. Wang, S. F. et al. Proteome of mouse oocytes at different developmental stages. *P Natl Acad. Sci. USA* **107**, 17639–17644 (2010).
43. Gao, Y. et al. Protein expression landscape of mouse embryos during pre-implantation development. *Cell Rep.* **21**, 3957–3969 (2017).
44. Palmerola, K. L. et al. Replication stress impairs chromosome segregation and preimplantation development in human embryos. *Cell* **185**, 2988–3007.e2920 (2022).
45. Bui, H. T. et al. Effect of trichostatin A on chromatin remodeling, histone modifications, DNA replication, and transcriptional activity in cloned mouse embryos. *Biol. Reprod.* **83**, 454–463 (2010).
46. Boutros, R., Dozier, C. & Ducommun, B. The when and wheres of CDC25 phosphatases. *Curr. Opin. Cell Biol.* **18**, 185–191 (2006).
47. Boutros, R., Lobjois, V. & Ducommun, B. CDC25 phosphatases in cancer cells: key players? Good targets? *Nat. Rev. Cancer* **7**, 495–507 (2007).
48. Ray, D. et al. Hemizygous disruption of Cdc25A inhibits cellular transformation and mammary tumorigenesis in mice. *Cancer Res* **67**, 6605–6611 (2007).
49. Chen, M. S., Hurov, J., White, L. S., Woodford-Thomas, T. & Piwnica-Worms, H. Absence of apparent phenotype in mice lacking Cdc25C protein phosphatase. *Mol. Cell Biol.* **21**, 3853–3861 (2001).
50. Lincoln, A. J. et al. Cdc25b phosphatase is required for resumption of meiosis during oocyte maturation. *Nat. Genet* **30**, 446–449 (2002).
51. Pirino, G., Wescott, M. P. & Donovan, P. J. Protein kinase A regulates resumption of meiosis by phosphorylation of Cdc25B in mammalian oocytes. *Cell Cycle* **8**, 665–670 (2009).
52. Kim, J. et al. LSD1 is essential for oocyte meiotic progression by regulating CDC25B expression in mice. *Nat. Commun.* **6**, 10116 (2015).
53. Ferencova, I. et al. CDC25B is required for the metaphase I-metaphase II transition in mouse oocytes. *J. Cell Sci.* **135**, jcs252924 (2022).
54. Cui, C., Zang, T. X., Cao, Y., Qin, X. & Zhang, X. W. CDC25B is involved in the centrosomal microtubule nucleation in two-cell stage mouse embryos. *Dev. Growth Differ.* **58**, 714–726 (2016).
55. Kohama, Y., Saito, M., Yada, M. & Sakurai, H. Regulation of the stability and activity of CDC25A and CDC25B by protein phosphatase PP2A and 14-3-3 binding. *Cell Signal* **54**, 10–16 (2019).
56. Matthews, H. K., Bertoli, C. & de Bruin, R. A. M. Cell cycle control in cancer. *Nat. Rev. Mol. Cell Biol.* **23**, 74–88 (2022).
57. Millar, J. B. A. & Russell, P. The cdc25 M-phase inducer: an unconventional protein phosphatase. *Cell* **68**, 407–410 (1992).
58. Russell, P. & Nurse, P. Cdc25+ functions as an inducer in the mitotic control of fission yeast. *Cell* **45**, 145–153 (1986).
59. Lopez-Girona, A., Furnari, B., Mondesert, O. & Russell, P. Nuclear localization of Cdc25 is regulated by DNA damage and a 14-3-3 protein. *Nature* **397**, 172–175 (1999).
60. Bulavin, D. V. et al. Initiation of a G2/M checkpoint after ultraviolet radiation requires p38 kinase. *Nature* **411**, 102–107 (2001).
61. Roy, M. J. et al. Structural mapping of PEAK pseudokinase interactions identifies 14-3-3 as a molecular switch for PEAK3 signaling. *Nat. Commun.* **14**, 3542 (2023).
62. Torosyan, H. et al. Structural insights into regulation of the PEAK3 pseudokinase scaffold by 14-3-3. *Nat. Commun.* **14**, 3543 (2023).
63. Lu, M. S. & Prehoda, K. E. A NudE/14-3-3 Pathway Coordinates Dynein and the Kinesin Khc73 to Position the Mitotic Spindle. *Dev. Cell* **26**, 369–380 (2013).
64. Uchida, S. et al. Binding of 14-3-3β but not 14-3-3σ controls the cytoplasmic localization of CDC25B: binding site preferences of 14-3-3 subtypes and the subcellular localization of CDC25B. *J. Cell Sci.* **117**, 3011–3020 (2004).
65. De, S. & Kline, D. Evidence for the requirement of 14-3-3eta (YWHAH) in meiotic spindle assembly during mouse oocyte maturation. *BMC Dev. Biol.* **13**, 10 (2013).
66. Meng, J. et al. The Role of 14-3-3ε Interaction with Phosphorylated Cdc25B at Its Ser321 in the Release of the Mouse Oocyte from Prophase I Arrest. *Plos One* **8**, e53633 (2013).
67. Gohla, A. & Bokoch, G. M. 14-3-3 regulates actin dynamics by stabilizing phosphorylated cofilin. *Curr. Biol.* **12**, 1704–1710 (2002).

68. Sztein, J. M., Farley, J. S. & Mobraaten, L. E. In vitro fertilization with cryopreserved inbred mouse sperm. *Biol. Reprod.* **63**, 1774–1780 (2000).
69. Scheres, S. H. W. RELION: Implementation of a Bayesian approach to cryo-EM structure determination. *J. Struct. Biol.* **180**, 519–530 (2012).
70. Zheng, S. Q. et al. MotionCor2: anisotropic correction of beam-induced motion for improved cryo-electron microscopy. *Nat. Methods* **14**, 331–332 (2017).
71. Zhang, K. Gctf: Real-time CTF determination and correction. *J. Struct. Biol.* **193**, 1–12 (2016).
72. Pettersen, E. F. et al. UCSF ChimeraX: Structure visualization for researchers, educators, and developers. *Protein Sci.* **30**, 70–82 (2021).
73. Adams, P. D. et al. Phenix: a comprehensive Python-based system for macromolecular structure solution. *Acta Crystallogr D. Biol. Crystallogr* **66**, 213–221 (2010).
74. Emsley, P., Lohkamp, B., Scott, W. G. & Cowtan, K. Features and development of Coot. *Acta Crystallogr D. Biol. Crystallogr* **66**, 486–501 (2010).
75. Dai, X. X. et al. PABPN1 functions as a hub in the assembly of nuclear poly(A) domains that are essential for mouse oocyte development. *Sci. Adv.* **8**, eabn9016 (2022).
76. Picelli, S. et al. Full-length RNA-seq from single cells using Smart-seq2. *Nat. Protoc.* **9**, 171–181 (2014).
77. Ma, J. et al. iProX: an integrated proteome resource. *Nucleic Acids Res.* **47**, D1211–D1217 (2019).
78. Chen, T. et al. iProX in 2021: connecting proteomics data sharing with big data. *Nucleic Acids Res.* **50**, D1522–D1527 (2022).

Acknowledgements

We are grateful to the staff from the Cryo-EM Facility of SKLB West China Cryo-EM Center of Sichuan University and The Kobilka Cryo-Electron Microscopy Center of The Chinese University of Hong Kong (Shenzhen) for the Cryo-EM support. We thank National Key Laboratory of Crop Genetic Improvement of Huazhong Agricultural University and Prof Lunzhi Dai and Zhili Xia from State Key Laboratory of Biotherapy, Sichuan University for the support of mass spectrometry determination and analysis. We thank Qingting Liu and Jinhong Li for help with recombinant protein expression and purification. We thank Jiying Zhang for coordination of ITC assays. The research leading to these results was funded by (1) the National Natural Science Foundation of China (No. 31930033 to L.L., 31971132 to D.D., and 31871449 to J.C.); (2) National Key R&D Program of China (2022YFC2702201) to L.L.; (3) Strategic Collaborative Research Program of the Ferring Institute of Reproductive Medicine (180202) to L.L. Z.H. was supported by the Fundamental Research Funds for the Central Universities (SCU2023G4175). R.W. was funded by High-level talent introduction project of Yunnan Provincial First People's Hospital (KHYJ-2023-5-04) and Yunnan Fundamental Research Projects (202401CF070009).

Author contributions

Z.H., L.L., and D.D. designed experiments and methods for data analysis. Z.H. performed all experiments and analyzed the data, with the following exceptions: R.W. performed in vitro transcription and microinjection of oocytes and zygotes. P.C. performed expression and purification of recombinant protein complexes and prepared cryo-EM samples. L.M. and Z.Z. were responsible for human GV oocytes collection from fresh ovarian tissues. Y.L. was responsible for collecting discarded human embryos during routine IVF and in vitro culture procedures. Z.Z. and R.W were responsible for murine oocytes and zygotes collection. Z.Z. performed IVF and the detection of DNA synthesis in embryos. Cryo-EM data acquisition and analysis workflow were established by H.J., and J.L., P.C., and X.W. participated in model building and refinement of the map of SCMC-14-3-3γ. Pull-down and Co-IP assays were done by Z.H., P.C., Z.Z., G.O., and Q.Q., with the exception of partial results in Fig. 1a (Co-IP assay of TLE6) done by R.W. Immunoblotting assays were done by Z.H., R.W., Z.Z., and G.O., with the exception of the results in Fig. 4d performed by Q.Q. The results in Fig. 6b,c,e,f were done by Z.Z and L.M. The results in Supplementary Fig. 7c were done by D.Z. Z.Z., D.Q., C.X., D.Z., Y.L., L.M., X.Y., and Z.G. participated in experiments on mouse oocytes or zygotes and assisted with data analysis. X.W., J.C., H.H., L.L., and D.D. participated in structural and biochemical data analysis, experiment design and fundings. Z.H., Z.Z., L.L., and D.D. wrote the manuscript and prepared the Figures, with the exception of Figs. 2f, 3a,e,i–l and 5a,i and Supplementary Figs. 7,10d,11,12, and 17a,b prepared by R.W. and D.Z.; Figs. 1c–e and 2a–c and Supplementary Figs. 1a,b,d, 3, and 4 prepared by P.C.; Supplementary Fig. 2 and Supplementary Table 1 prepared by H.J. and X.W. The manuscript and Figures were prepared with input from all authors. L.L. and D.D. conceived and supervised the study.

Competing interests

The authors declare no competing interests.

Additional information

Supplementary information The online version contains supplementary material available at https://doi.org/10.1038/s41467-024-53277-3.

Correspondence and requests for materials should be addressed to Lei Li or Dong Deng.

Peer review information *Nature Communications* thanks Chun So, and the other, anonymous, reviewer(s) for their contribution to the peer review of this work. A peer review file is available.